ISSP

Activity Report A 2001

Contents

PREFACE

- Activity Report A -

ISSP was established in 1957 based on the recommendation of the National Council of Japan to promote the cooperative research throughout the country in condensed matter physics in close contact with other related fields of science such as chemistry and earth science on one hand and to pursue its own scientific research on the other hand. This foreseeing philosophy of the founders together with the constant efforts afterwards had made ISSP very active in both ways in recent years, especially after the introduction of the large group system in 1980 and the moving to the new campus of Kashiwa. So far there were various forms of the publications to make the status of the research activity of ISSP public. New forms are now introduced; the Activity Reports A and B, which show the up-to-date status of these scientific activities in separate ways depending on the styles of the pursuing the research. This Activity Report A is based on the research activity of the staffs of the ISSP in the fiscal year of 2001. In the first half about 30 topics are reported as the highlights, whereas in its second half a brief summary of scientific activities and all publications of each research groups of ISSP are listed.

We are happy to receive any comments on the Report for the possible improvement of the overall research activity of ISSP.

August 19, 2002

Hidetoshi Fukuyama

Director
Institute for Solid State Physics
The University of Tokyo

Observation of Quantized Plateaux and Magnetic Superstructures in a 2D Spin System $SrCu_2(BO_3)_2$ under High Fields

M. Takigawa, Y. Ueda and T. Goto

The discovery of a spin-gap and magnetization plateaux in $SrCu_2(BO_3)_2$ [1] stimulated tremendous amount of experimental and theoretical activities. The crystal structure realizes a stack of the two-dimensional Shastry-Sutherland spin model [2] (Fig. 1), for which a direct product of dimer singlets is known to be the exact ground state. A remarkable property of this material is the magnetization under high fields, which exhibits plateaux at fractional values (1/8, 1/4 and 1/3) of the fully saturated Cu moment.

However, the previous magnetization curve up to 58 T was far from saturation and thus one could not answer the question of, e.g., the existence of the 1/2 plateau under theoretical debates. In 2001, we developed magnets at High Magnetic Field Laboratory, KYOKUGEN in Osaka University and performed the magnetization experiment to 69 T, where a single crystal grown by a traveling solvent floating zone technique was used. The result for H // c at 1.3 K in Fig. 1 has revealed that, although magnetic field is still not enough to get full magnetization, the 1/3 plateau survives in a range at least as wide as 25 T, meaning that this plateau is much more stable than the 1/4 and 1/8 plateaux. Within the experimental accuracy, no hysteretic behavior is observed between field increasing and decreasing scans.

Another challenging issue is the observation of magnetic superstructures at the plateaux. Theories based on the hard core boson model have predicted simple commensurate superstructures of triplets. Whereas some superstructures at 1/8, for example, are proposed as shown in Fig. 2, there has been no experimental evidence so far. NMR is best suited to detect magnetic superstructure at high magnetic field. In June 2000, we have first performed NMR experiments for ^{11}B nuclei up to 28 T using a 20MW resistive magnet at Grenoble High Magnetic Field Laboratory in the temperature range above 1.5 K. The field range covers the 1/8 magnetization plateau that occurs above 27 T. Although we observed non-trivial spin dynamics at high field, no indication of static spin structure associated with the 1/8-plateau was obtained. We then continued NMR experiments in May and November 2001 for both ^{11}B and $^{63,65}Cu$ nuclei at a

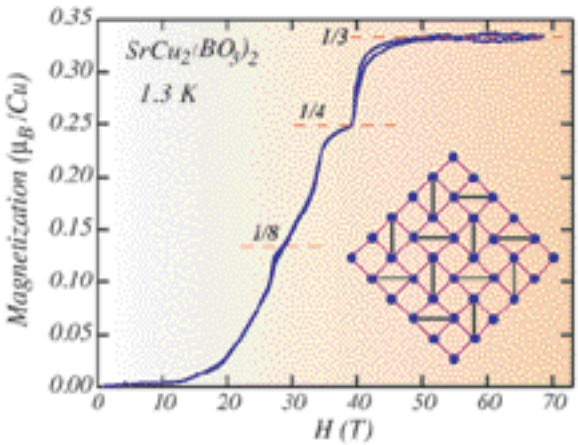

Fig. 1. Magnetization curve of $SrCu_2(BO_3)_2$ up to 69 T at 1.3 K. The 1/8, 1/4 and 1/3 plateaux are observed. The Shastry-Sutherland model is shown in the inset.

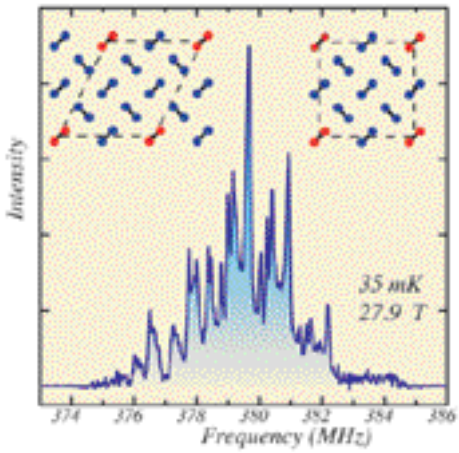

Fig. 2. NMR spectrum of ^{11}B nuclei in $SrCu_2(BO_3)_2$ at 27.9 T and 35 mK. Inset shows the superstructures at the 1/8 plateau proposed based on the hard core boson approximation, where dumbbells in blue represent singlets and those in red triplets.

much lower temperature of 35 mK. We observed a drastic change of the ^{11}B NMR spectrum as shown in Fig. 2. A single peak for each of the quadrupole-split three resonance lines observed at 26 T is transformed to multiple-peak structure at 27.9 T. The former is consistent with the uniformly magnetized state, while the latter provides firm microscopic evidence for a spatially modulated magnetic superstructure at the 1/8-plateau. The spectrum at 27.9 T contains peaks with both positive and negative magnetic hyperfine shifts, suggesting that while most Cu spins point along the magnetic field, some spins are polarized opposite to the field. This contradicts the superstructures in Fig. 2 and indicates an artifact of the hard core boson approximation. Triggered by our experiment, Miyaraha *et al.* proposed a new approach starting from the original Heisenberg spin Hamiltonian with adiabatic spin-phonon coupling and succeeded to reproduce quantitatively the magnetization superstructure with a rhomboid unit cell and Friedel-like oscillation. This result will be reported elsewhere soon.

References
[1] H. Kageyama *et al.*, Phys. Rev. Lett. **82**, 3168 (1999).
[2] S. Miyahara and K. Ueda, Phys. Rev. Lett. **82**, 3701 (1999).

Authors
M. Takigawa, K. Kodama, H. Kageyama, Y. Ueda, T. Goto, M. Horvatic[a], C. Berthiera[a], Y. Narumi[b], K. Kindo[b]
[a]CNRS and MPI-FKF, Grenoble, France.
[b]Osaka University.

Superconductivity at 1 K in Frustrated Pyrochlore Oxide $Cd_2Re_2O_7$

Z. Hiroi, T. Sakakibara and M. Takigawa

Frustration is one of the most interesting topics in the field of solid state physics. Generally, it suppresses long-range order of spins or charges on lattice points and tends to stabilize a novel quantum-disordered state. The playground is triangle-based lattices like a two-dimensional Kagome lattice or a three-dimensional pyrochlore lattice (Fig. 1). Pyrochlore oxides are typical transition-metal oxides comprising the latter lattice. Although many metallic pyrochlore oxides are known, no superconductivity has been observed

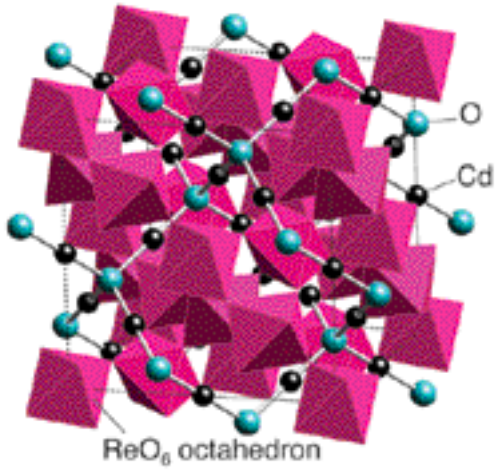

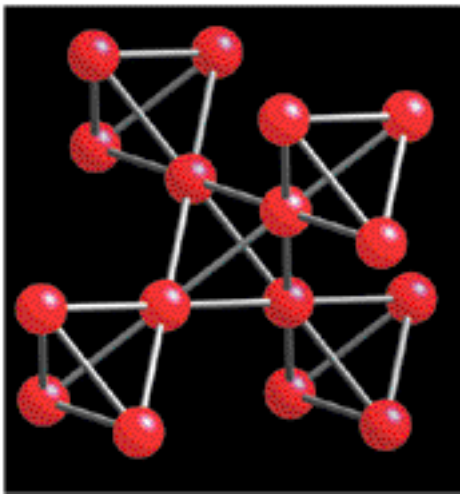

Fig. 1. Crystal structure of $Cd_2Re_2O_7$ (top). Pink octahedra representing the ReO_6 unit are linked to each other by their corners. When only Re or Cd atoms are extracted from the structure, the pyrochlore lattice made of corner-sharing tetrahedra appears (bottom). Red balls represent Re or Cd atoms.

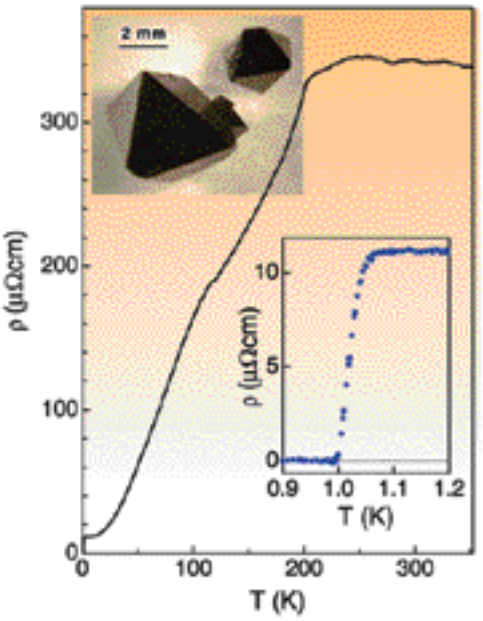

Fig. 2. Resistivity showing a superconducting transition at T_c = 1.0 K. The anomalies at 200 K and 120 K are due to structural phase transitions where the pyrochlore structure are deformed slightly in two steps. The inset shows the photo of grown single crystals used for various measrements.

so far. We report here the first pyrochlore oxide superconductor $Cd_2Re_2O_7$.

We have prepared single crystals of $Cd_2Re_2O_7$ (inset to Fig. 2) and measured resistivity, magnetic susceptibility, and specific heat down to T = 0.4 K. Surprisingly observed at 1 K is a sharp drop in resistivity (Fig. 2), a large diamagnetic signal in magnetization, and a well-defined λ-type anomaly in specific heat. These experimental facts give a strong evidence for the occurrence of superconductivity. In addition, we observed two successive phase transitions at 200 K and 120 K where resistivity shows anomalies (Fig. 2). They are very intriguing, probably related to charge, spin, and orbital degrees of freedom for Re ions with two 5*d* electrons. We expect a novel physics involved in this compound on the basis of frustration on the pyrochlore structure.

Principal Publication and Authors

M. Hanawa, Y. Muraoka, T. Tayama, T. Sakakibara, J. Yamaura and Z. Hiroi; Phys. Rev. Lett. **87**, 187001 (2001).

Superconductivity and magnetic fluctuations in $Cd_2Re_2O_7$ via Cd NMR and Re NQR

M. Takigawa and Z. Hiroi

The pyrochlore oxides has the chemical formula $A_2B_2O_7$, where both A and B sites form a network of corner-sharing tetrahedra, known as the pyrochlore lattice. Localized magnetic moments on a pyrochlore lattice has attracted enormous recent interest since strong geometrical frustration inhibits conventional Neel order, resulting in exotic ground states. In itinerant electron systems, geometrical effects are not as well understood as the case of insulating magnets. However, recent discovery of superconductivity with $T_c \sim 1$ K and successive structural phase transitions at T_{s1} = 200 K and T_{s2} = 120 K in $Cd_2Re_2O_7$ by Hiroi group at ISSP have opened new opportunities to investigate the role of lattice geometry in various electronic phases. (See the previous article.)

We have performed nuclear magnetic resonance (NMR)

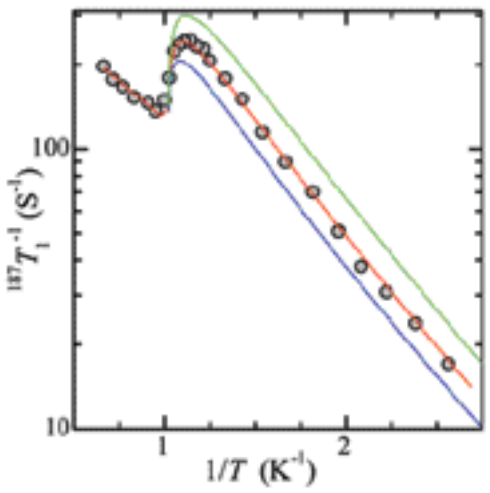

Fig. 1. The spin-lattice relaxation rate ($1/T_1$) of ^{187}Re nuclei near and below the superconducting transition temperature (1 K) measured by NQR at zero magnetic field is plotted against inverse temperature ($1/T$). The lines show the results of weak coupling BCS theory assuming a uniform distribution of the energy gap between $\Delta - \delta$ and $\Delta + \delta$ where Δ is the average gap. The red, blue and green lines indicates the results for δ / Δ = 0.22, 0.27, and 0.17, respectively.

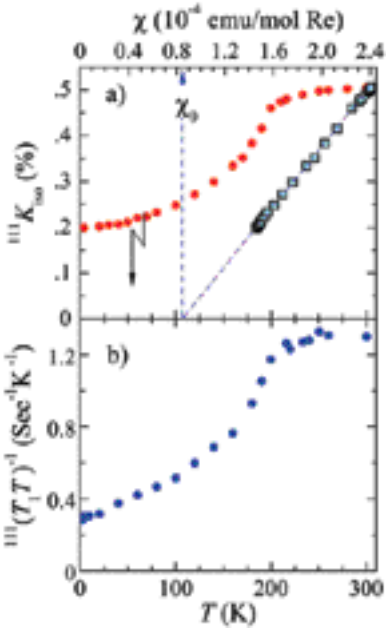

Fig 2. a) The isotropic part of the Knight shift for ^{111}Cd nuclei is plotted against temperature (red, lower scale) or magnetic susceptibility (blue, upper scale). b) The temperature dependence of $(T_1T)^{-1}$ for ^{111}Cd nuclei, indicating steep decrease of the density of states below the structural transition at 200 K.

and nuclear quadrupole resonance (NQR) experiments on $Cd_2Re_2O_7$ to obtain microscopic insight on the superconducting, structural and magnetic properties [1, 2]. The pronounced coherent peak and the activated temperature dependence of the spin-lattice relaxation rate at the Re sites in the superconducting state shown in Fig. 1 provide strong evidence for weak coupling BSC behavior with a nearly isotropic energy gap.

A sharp single set of NQR lines at the Re sites rules out any magnetic or charge order down to 0.4 K. The electric field gradient (EFG) at the Re sites as revealed from NQR spectra does not possess axial symmetry, imposing that the crystal structure is not cubic below T_{s1} = 200 K. This has been confirmed by subsequent various diffraction experiments. The NQR spectrum also shows discontinuous change near T_{s2} = 120 K confirming the first order structural transition in addition to the second order transition at T_{s1}.

The static and dynamic magnetic properties were investigated by NMR measurements for the Cd sites using a single crystal as shown in Fig. 2. The steep reduction of the Knight shift (spin susceptibility) and $(T_1T)^{-1}$ below 200 K indicate that the structural distortion at T_{s1} causes significant loss of the density of states (DOS). Thus the transition at T_{s1} is characteristic of a Peierls transition or band Jahn-Teller effects. This appears to have common physics with insulating magnets in which lattice distortion occurs to gain magnetic energy by eliminating frustration of exchange interactions and reducing the ground state degeneracy. On the other hand, little anomalies were observed at T_{s2} for thermodynamic properties, where local structure as revealed NQR spectrum shows pronounced discontinuity. What drives the transition at T_{s2} still remains a puzzle.

References
[1] O. Vyaselev *et al*. phys. Rev. Left. **89**, 017001 (2002).
[2] K. Arai *et al*. J. Phys. Condens. Matter **14**, L461 (2002).

Authors
O. Vyaselev, K. Arai, K. Kobayashi, J. Yamazaki, K. Kodama, M. Takigawa, M. Hanawa and Z. Hiroi

Observation of Coherent Magnon Oscillation in Sodium Vanadate

T. Suemoto and Y. Ueda

Sodium Vanadate : The sodium vanadate α'-NaV_2O_5 shows a spin-Peierls-like phase transition at T_c = 34 K [1]. Below T_c, this compound exhibits charge ordering with alternating V^{4+} and V^{5+} ions accompanied by a lattice distortion[2]. The spins attached to V^{4+} ions are believed to be dimerized with anti-parallel orientations in a zig-zag configuration[3]. The dimerized spin system reveals unique magnetic excitation spectra consisting of a triplet branch at the gap energy Δ, a corresponding two-particle continuum of spin excitations starting from 2Δ, and well defined magnetic bound states between Δ and 2Δ.

Coherent excitation method : Owing to the recent development of the femtosecond lasers, time domain spectroscopy has become to be a versatile tool for investigating low energy excitations in solids. By probing the small modulation of the reflectivity after impulsive excitation by using ultra-short pulses, we can observe the oscillation of lattice or any other elementary excitations on femtosecond (10^{-15} sec) time scale, just like electric signals we can watch on an oscilloscope. Observation of phonons or plasmons has been reported for many typical semiconductors and some oxides. However, this method has not been applied for probing magnons.

We carefully chosen a small flat area on a cleaved α'-NaV_2O_5 sample and irradiated it by 25 fs pump pulses in a 40 μm spot as shown in Fig. 1. A probe pulse with an appropriate delay time hits the same area from a slightly different direction and the modulation in the reflected light intensity (actually the difference in two perpendicular polarizations) was analyzed by a lock-in amplifier.

Two magnon oscillation at 127 cm^{-1} : The inset of Fig. 2 shows the raw data which is an oscillation signal as a function of delay time. In the Fourier transformed spectrum shown in the same figure, we found a new excitation peak at 127 cm^{-1} [2] in addition to well known phonon lines at higher frequencies. In spite of extensive Raman work, this peak has never been reported before. This peak has been observed only with circularly polarized light and shows a temperature dependence characteristic to magnetic excitation. Based on these facts, we assigned this peak to one of the triplet two

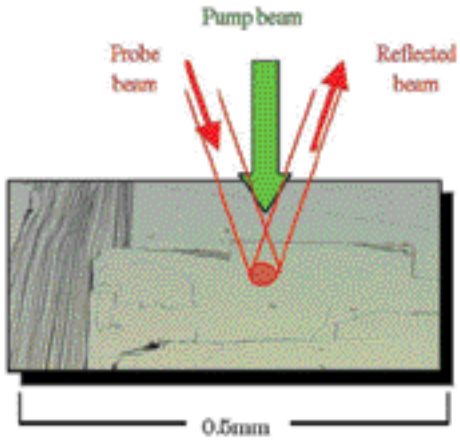

Fig. 1. Microscope image of the sample surface. The red shaded area is excited by the pump pulse (Thick green arrow) and the reflectance is probed by the other pulse (red arrows)

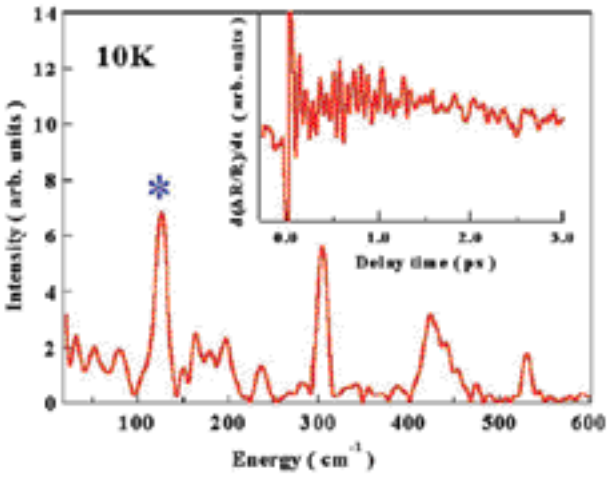

Fig. 2. The time response of the reflection signal (inset) and its Fourier transform. The peak indicated by an asterisk corresponds to a newly found two magnon bound state.

magnon bound states, which have been theoretically expected to appear below the two magnon continuum [3].

This demonstrates the generation of coherent magnetic excitation and the usefulness of "femtosecond spectroscopy" for investigating the "strongly correlated electron systems".

References
[1] M. Isobe and Y. Ueda, J. Phys. Soc. Jpn. **65**, 1178 (1996).
[2] T. Ohama, H. Yasuoka, M. Isobe and Y. Ueda, Phys. Rev. B**59**, 3299 (1999).
[3] H. Seo and H. Fukuyama, J. Phys. Soc. Jpn. **67**, 2602 (1998).
[4] H. Kamioka, S. Saito, M. Isobe, Y.Ueda and T. Suemoto, Phys. Rev. Lett. **88** 127201 (2002).
[5] S. Trebst *et al*, Phys. Rev. Lett. **85** 4373 (2000).

Authors
H. Kamioka, S. Saito, T. Suemoto, M. Isobe and Y. Ueda

"Devil's Flower" Blooming in NaV_2O_5

Y. Fujii and Y. Ueda

The most exciting phase diagram in statistical physics - ***Devil's flower*** [1] - has been reproduced experimentally in Temperature-Pressure (*T*-*P*) phase diagram of NaV_2O_5[2].

A quarter-filled spin-ladder system NaV_2O_5 undergoes a

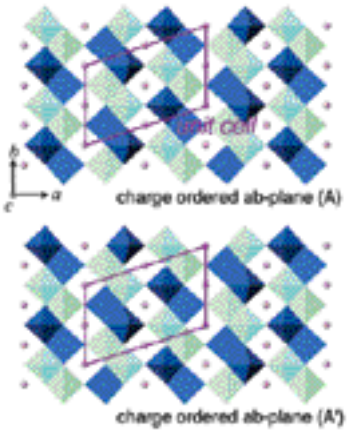

Fig. 1. Schematic charge order pattern determined in ab-plane, consisting two kinds of patterns A and A'. One charge localizes in the blue pyramid of $V^{4+}O_5$. The charge and corresponding lattice modulation along the *c*-axis are determined by the combination of A and A'. For example, AAA'A' for $2a \times \sim 2b \times \sim 4c$ superstructure below

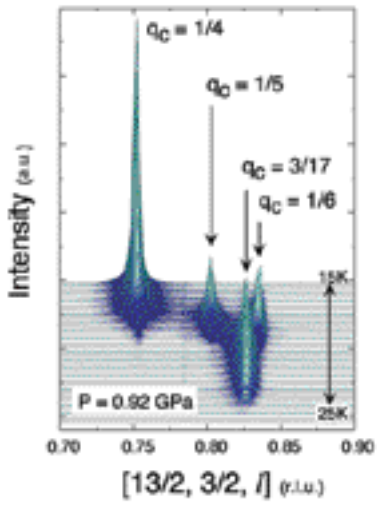

Fig. 2. Temperature dependence of high-resolution x-ray diffraction profiles observed along the [13/2, 3/2, q_c] direction at 0.92 GPa. One can clearly see a series of superlattice reflections with q_c = 1/4, 1/5, 1/6 and 3/17 which systematically appear and disappear as a function of temperature.

novel cooperative phase transition at T_c = 34K associated with its charge ordering, lattice dimerization ($2a \times \sim 2b \times \sim 4c$ superstructure) and spin-gap formation. By the complementary use of synchrotron x-ray structural analysis and resonant x-ray scattering (RXS) techniques at Photon Factory, the $2a \times \sim 2b \times \sim 4c$ superstructure below T_c was solved unambiguously[3,4]. A oblique charge stripe pattern formed in each V_2O_5-layer (*ab*-plane) is shown in Fig. 1 as A and A'. Atomic shifts coupled with such a charge ordering are not shown in this figure. The charge ordering patterns called A and A' are related by a phase shift by π along the *b*-axis, where a dark blue colored pyramid represents $V^{4+}O_5$ and a light blue $V^{5+}O_5$. The stacking sequence of the patterns A and A' along the c-axis was unambiguously determined by the RXS as AAA'A' [4].

By application of high pressure, the stacking sequence along the *c*-axis drastically changes. Figure 2 displays temperature dependence of high-resolution diffraction profiles observed along the [13/2, 3/2, q_c] direction at 0.92 GPa. In this figure a few more reflections are newly observed and one can clearly see a series of superlattice reflections with q_c = 1/4, 1/5, 1/6 and 3/17 which systematically appear and disappear as a function of temperature. What we observe is

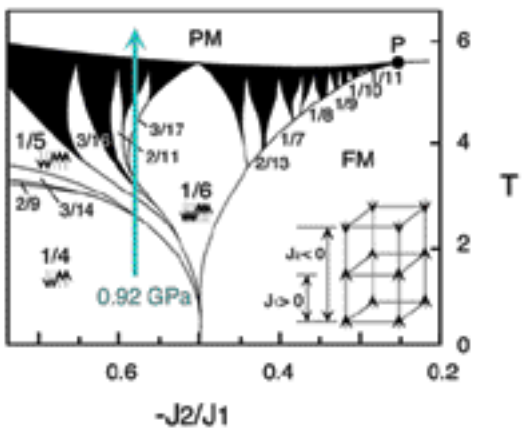

FIg. 3. "*Devil's Flower*" obtained from the ANNNI model. The blue arrow represents the tracing path corresponding to the temperature variation of the experiment shown in Fig. 2.

peak intensities coming from the atomic shifts; however, the charge also modulates with the same modulation wave number q_c[5]. This q_c sequence means that the stacking sequence along the *c*-axis drastically changes as AAA'A'A' for 1/5, AAAA'A'A' for 1/6, AAA'A'A'AAAA'A'A'AAAA'A'A' for 3/17 and so on.

The observed q_c sequence is well understood by the "Devil's Staircase" type sequence theoretically obtained from the Axial Next Nearest Neighbor Ising (ANNNI) model proposed by Bak & von Boehm[1]. Fig. 3 shows the T versus $-J_2/J_1$ phase diagram very well known as "***Devil's Flower***". The green arrow corresponds to the scanning path of Fig. 2, i.e. temperature variation at a fixed pressure 0.92 GPa. We observed the other types of q_c sequences in a wide temperature and pressure range and finally confirmed that the "***Devil's Flower***" is perfectly reproduced in NaV_2O_5 [2] under high pressure. A microscopic mechanism of the competitive inter-layer interaction resulting in such a phase diagram is a keen subject to further study.

References

[1] P. Bak *et al*. Phys. Rev. B **21**, 5297 (1980)
[2] K. Ohwada *et al*. Phys. Rev. Lett. **87**, 086402 (2001).
[3] H. Sawa *et al*. J. Phys. Soc. Jpn. **71**, 385 (2001).
[4] Y. Katsuki, Master Thesis (Graduate School of Science, The University of Tokyo, Mar. 2002); Y. Fujii *et al*. in preparation.
[5] K. Ohwada *et al*. private communication.

Authors

K. Ohwada*, Y. Katsuki**, Y. Fujii, M. Isobe, Y. Ueda, H. Nakao[a], Y. Murakami[a], E. Ninomiya[b], and H. Sawa[c]
*Present address: JAERI/SPring-8. **Present address: Accenture Co. Ltd. [a]Tohoku University, [b]Chiba University, [c]KEK-PF

Discovery of Missing Link: I. A Superconducting Vanadate β -$Na_{0.33}V_2O_5$

Y. Ueda

Since the discovery of high-T_C superconducting cuprates, the superconductivity has drawn much interest as the ground state of strongly correlated electron systems. Vanadium element has also carried many metallic oxides; nevertheless superconductivity has never been found in vanadium oxides. Many metallic vanadium oxides show metal-insulator (M-I) transitions as a function of temperature and the ground states of them are magnetic insulators.

The quasi-one-dimensional conductor β -$Na_{0.33}V_2O_5$ with a mixed-valence of V^{4+}/V^{5+} = 1/5 exhibits a M-I transition of a charge ordering type at T_{CO} = 135K and the charge-ordered structure undergoes an antiferromagnetic transition at T_N = 25 K. This M-I transition (charge order transition) is suppressed by hydrostatic pressure and the superconducting phase with T_{SC} = 9 K appears around P=8GPa where the charge ordered phase collapses. This is the first observation of superconductivity in vanadium oxides and also the first observation of a phase transition from charge ordered phase to superconducting phase.

Competition of ground states in many-body electron system is a central problem in condensed matter physics. It is described as a phase diagram in the thermodynamic parameters space such as temperature vs. pressure or magnetic field. Several exotic phase diagrams including superconducting phases have been observed in various compounds such as inter 4*f*/5*f* metallic alloys, organic conductors and high-T_c superconducting cuprates. The obtained phase diagram (Figure 1) is independent of those phase diagrams. The superconducting phase is adjacent to the charge ordered phase in β-$Na_{0.33}V_2O_5$, while it is adjoined the magnetic ordered phases in the inter 4*f*/5*f* metallic alloys and organic conductors. This suggests an important role of charge fluctuation for the superconductivity in β -$Na_{0.33}V_2O_5$.

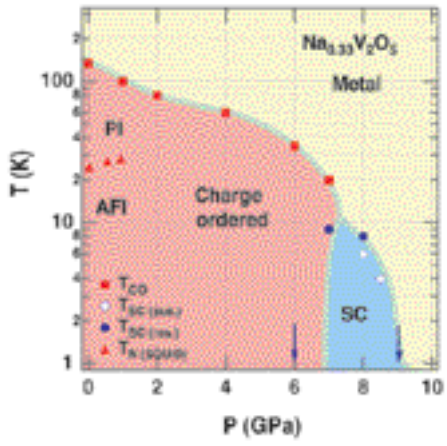

Fig.1. Pressure-temperature (*P*-*T*) phase diagram of β -$Na_{0.33}V_2O_5$. With increasing pressure the charge ordering temperature (T_{CO}) decreases and the Néel temperature (T_N) increases, and beyond P = 7 GPa the superconducting phase (SC) appears. This is the first observation of superconductivity in vanadium oxides. The superconducting transition temperature (T_{SC}) decreases with further increase of pressure and finally the superconducting phase disappears above P = 9 GPa. In β -$Na_{0.33}V_2O_5$ the superconducting phase competes with the charge ordered phase, which suggests an important role of charge fluctuation for the superconductivity.

Principal publication and authors

T. Yamauchi, Y. Ueda and N. Môri, PRL **89** 057003 (2002).

First-order Transition at the Upper Critical Field in the Heavy Electron Superconductor $CeCoIn_5$

T. Sakakibara

The tetragonal heavy electron compound $CeCoIn_5$ becomes superconducting at T_c = 2.3 K. Various experimen-

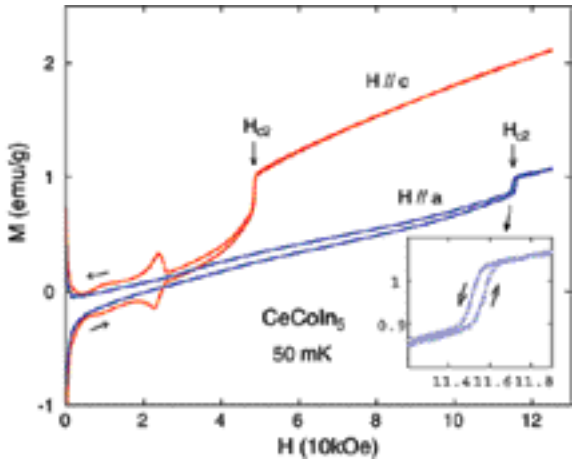

Fig.1. Magnetization curves of $CeCoIn_5$ measured at T = 50 mK, with magnetic field applied parallel to the tetragonal *a* and *c* axes. The sharp jump of the magnetization shows the H_{c2} transition is of first order. The inset shows the magnetization behavior near H_{c2} (H//a) in an expanded scale, revealing a small hysteresis in the transition field.

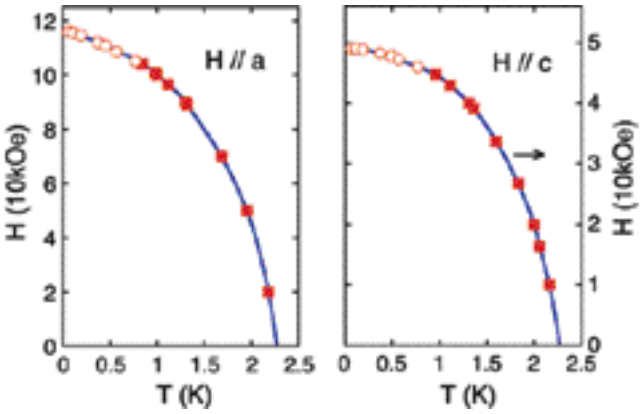

Fig. 2. Phase diagrams of $CeCoIn_5$ under magnetic field parallel to the *a* and *c* axes. Open circles are the first-order H_{c2} transition points where the magnetization shows a discontinuous jump, whereas the solid squares are the second-order one.

tal studies indicate that the electron pairing is even parity (spin singlet) with k_x^2-k_y^2 gap symmetry[1]. Due to its large Pauli paramagnetic susceptibility in the normal state, $CeCoIn_5$ provides an interesting situation where the paramagnetic energy becomes a substantial fraction of the superconducting condensation energy at high fields and may affect the upper critical field H_{c2} at low temperatures. We have examined the superconducting phase diagram of a single crystal of $CeCoIn_5$ (6.9 mg weight) by means of a low temperature DC magnetization measurement using a dilution refrigerator [2].

Figure 1 shows the magnetization curves obtained at the base temperature of 50 mK with slowly varying magnetic field applied parallel to the tetragonal *a* and *c* axes. The arrows indicate the direction of the field sweep. Very interestingly, the magnetization exhibits a discontinuous jump at H_{c2} for both field directions. This behavior is in striking contrast to the case of ordinary type-II superconductors in which the magnetization continuously recovers the normal state value at H_{c2}. Our results suggest that the H_{c2} transition in $CeCoIn_5$ is of first-order at low temperature. In fact, a small but distinct hysteresis is observed in the transition field (the inset of Fig.1).

We carried out the measurements at various temperatures. When the temperature was raised, the magnetization jump at H_{c2} became smaller and eventually vanished at around 0.7 K for both field directions. Figure 2 shows the resulting $H_{c2}(T)$ phase diagrams of $CeCoIn_5$. Open circles indicate the transition points which are considered to be of first order, whereas the solid squares denote the second order ones where the magnetization change is continuous. Thus, a critical point separating the first-order and the second-order transition lines seems to exist at $T \sim 0.3\ T_c$ for both field directions.

Although the origin of the first-order H_{c2} transition in $CeCoIn_5$ is not very clear at present, a promising mechanism will be the Pauli paramagnetic effect which comes from the difference in spin susceptibility between superconducting and normal states. The transition field to the normal state is suppressed at low temperature and may become of first order, provided that the spin paramagnetism is strong enough [3]. $CeCoIn_5$ might be the first system that exhibits a strong Pauli paramagnetic limiting of the upper critical field.

References
[1] K. Izawa *et al.*, Phys. Rev. Lett. **87** 057002 (2001) .
[2] T. Tayama *et al.*, Phys. Rev. B **65** 180504(R) (2002) .
[3] G. Sarma, J. Phys. Chem. Solids **24** 1029 (1963) .

Authors
T. Tayama, A. Harita, T. Sakakibara, Y. Haga[a], H. Shishido[b], R. Settai[b], and Y. Onuki[b]
[a]Advanced Science Research Center, Japan Atomic Energy Research Institute,Tokai, Ibaraki 319-1195.
[b]Graduate School of Science, Osaka University, Toyonaka, Osaka, 560-0043.

Giant Negative Magnetoresistance Originating from the d-π Interaction in a Molecule

H. Tajima

A search for a new function based on the interplay between local magnetic moments and conduction electrons is a current topic in the field of molecular conductors. Most of research works concern charge-transfer complexes composed of inorganic anions having local magnetic moments and molecular donors affording π- conduction electrons. The key to synthesize such compounds is the strength of the *d*-π interaction (the interaction between local magnetic moments and π- conduction electrons). In the case of the charge-transfer complexes above mentioned, however, this strength is determined by the crystal structure whose design is still beyond control. One of the ways to solve this problem is to synthesize charge transfer complexes by using the molecules, where the strong *d*-π interaction is self-contained. In this context, we have studied a new series of charge-transfer salts composed of the axial-substituted phthalocyanine (Pc), $[Fe^{III}(Pc)(CN)_2]^-$, in which the strong *d*-π interaction is self-contained. (See Fig. 1).

Figure 2 shows the temperature dependence of the resistivity for $TPP[Fe^{III}(Pc)(CN)_2]_2$ under the magnetic fields of 18 T and 0T [1, 2]. As can be seen from the figure, the resistivity drastically decreases under the applied magnetic field. The negative magnetoresistance in this salt is highly anisotropic for the magnetic-field orientation. This field-orientation dependence is consistent with that in the magnetic susceptibility. The Curie constant for *B*//*a* is more than 5-10

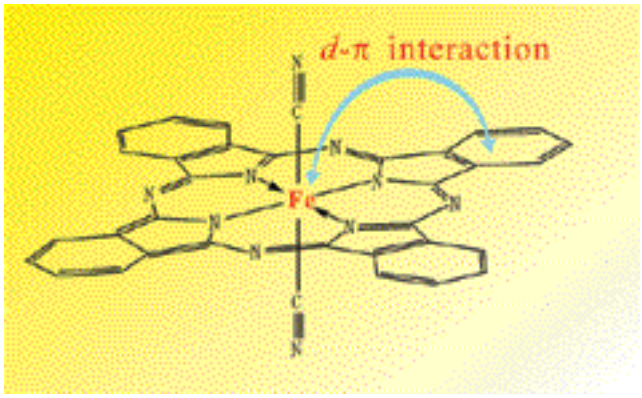

Fig. 1. Molecular structure of $[Fe^{III}(Pc)(CN)_2]^-$. In this molecule, *d*-electrons in Fe^{III} are the source of the local magnetic moment (S=1/2), and the π-electrons in the phthalocyanine (Pc) ring form the conduction band. The close contact between *d*- and π-orbitals gives rise to the strong d-π interaction inside the molecule.

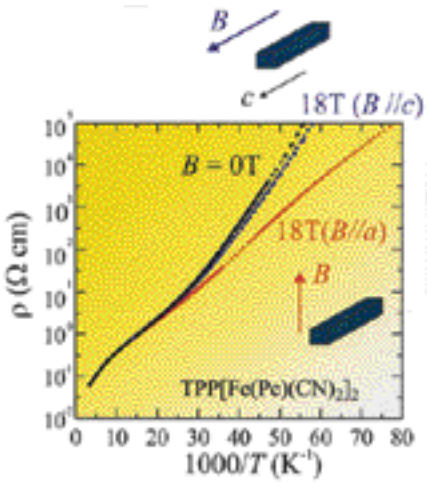

Fig. 2. Temperature dependence of the electrical resistivity under the magnetic field applied parallel to the *c*-and *a*-axis. The field-orientation dependence of the negative magnetoresistance is qualitatively consistent with the g-factor anisotropy in $[Fe^{III}(Pc)(CN)_2]^-$ unit.

times larger than that for *B*//*c*. Recently we determined the *g*-tensor of $[Fe^{III}(Pc)(CN)_2]^-$ using a model compound $\{(C_6H_5)_3P\}_2N[Fe^{III}(Pc)(CN)_2]$. (No ESR signal was observed for $TPP[Fe^{III}(Pc)(CN)_2]_2$.) The *g*-factors are g_1 = 3.6, g_2 = 1.1 and g_3 = 0.5, where g_1 denotes the *g*-factor for the static magnetic field approximately perpendicular to the Pc-ring, and g_2 and g_3 denote the two *g*-factors for the field approximately parallel to the Pc-ring [3]. Such large anisotropy in the *g*-factors is consistent with the field-orientation dependence of the giant negative magnetoresistance (and magnetic susceptibility) [4]. This strongly supports that the giant negative magnetoresistance in $TPP[Fe^{III}(Pc)(CN)_2]_2$ essentially originates from the *d*-π interaction in the $[Fe^{III}(Pc)(CN)_2]$ unit. In addition to $TPP[Fe^{III}(Pc)(CN)_2]_2$, we found the anisotropic giant negative magnetoresistance in $PTMA_x[Fe^{III}(Pc)(CN)_2]\cdot y(MeCN)$ [5] and $PXX[Fe^{III}(Pc)(CN)_2]$. Both compounds contain $[Fe^{III}(Pc)(CN)_2]$ unit.

References

[1] M. Matsuda, T. Naito, T. Inabe, N. Hanasaki, H. Tajima, T. Otsuka, K. Awaga, B. Narymbetov, and H. Kobayashi, J. Mater. Chem. **10**, 631 - 636 (2000).
[2] N. Hanasaki, H. Tajima, M. Matsuda, T. Naito, T. Inabe, Phys. Rev. B **62**, 5839 - 5842 (2000).
[3] N. Hanasaki, M. Matsuda, H. Tajima, T. Naito, T. Inabe, Synth. Met., in press.
[4] H. Tajima, N. Hanasaki, M. Matsuda, F. Sakai, T. Naito, T. Inabe, J. Solid State Chem., in press.
[5] M. Matsuda, T. Naito, T. Inabe, N. Hanasaki, H. Tajima, J. Mater. Chem. **11**, 2493 - 2497 (2001)

Authors
H. Tajima, N. Hanasaki, M. Matsuda, T. Naito[a], T. Inabe[a]
[a]Division of Chemistry, Graduate School of Science, Hokkaido University

First Systematic Band Filling Control in Organic Conductors

H. Mori

The systematic study of band filling control for four kinds of organic conductors with various kinds of ground states has been succeeded. (a) By partial substitution of $(GaCl_4^-)$ by (MCl_4^{2-}) [M = Co, Zn] in the anion blocking layer of λ-$ET_2(GaCl_4^-)$ [ET = bis(ethylenedithio)tetrathiafulvalene] [1], single crystals of λ-$ET_2(GaCl_4^-)_{1-x}(MCl_4^{2-})_x$

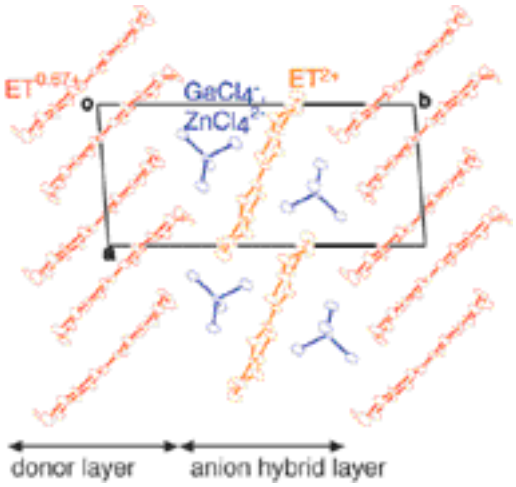

Fig. 1. Crystal structure of β'-$ET_3(ZnCl_4^{2-})_{2-x}(GaCl_4^{1-})_x$ [x=0.66]. The donor layer ($ET^{1-0.5x}$) and the anion hybrid layer [ET^{2+} and ($GaCl_4^{1-}$, $ZnCl_4^{2-}$)] stack alternately along the *b*-axis. The crystal structure analysis suggests that the carrier doping is performed mainly in the donor layer.

[x = 0.0, 0.05, 0.06] have been obtained. The resistivity at room temperature decreases from 3 ohm cm (x = 0.0) to 0.1 (x = 0.06) by doping to the antiferromagnet with an effective half-filled band (x = 0.0). (b) Another 2:1 (donor : anion) salt, δ-$ET_2(GaCl_4^-)$ which is a spin gap material, has been doped like δ'-$ET2(GaCl_4^-)_{1-x}(MCl_4^{2-})_x$ [x = 0.05, 0.14]. The resistivity is lowered from 10 ohm cm (x = 0.0) to 0.3 (x = 0.14). For both 2:1 salts, the semiconducting behaviors have transferred to relatively conductive semiconducting ones by doping. (c) As for *a*-type 3:1 salts, the parent material is in the charge ordering state like α-$(ET^+ET^+ET^0)(CoCl_4^{2-})$(TCE), where the charge-ordered donors are dispersed in the two-dimensional conducting layer. Although the calculation of α-$ET_3(CoCl_4^{2-})$(TCE) shows a band insulating nature, and the crystal structure analysis indicates that this material is in a charge-ordering state, the metallic behavior down to 165 K has been observed. With doping ($GaCl_4^-$) to the *a*-system, isostructural α-$ET_3(CoCl_4^{2-})_{1-x}(GaCl_4^-)_x$(TCE) [x = 0.54, 0.57, 0.62] have been afforded, where the pattern of the horizontal stripe-type charge ordering changes with an increase of x.

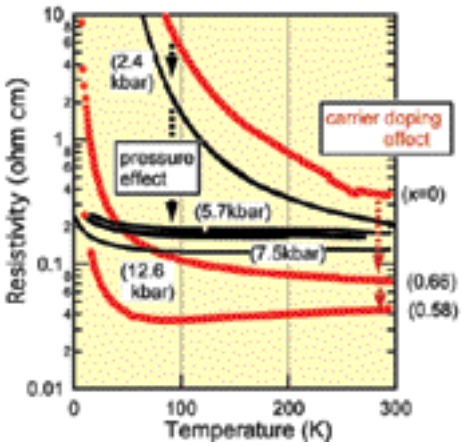

Fig. 2. Doping and pressure effect of β'-$ET3(ZnCl_4)^2$. The carrier doping makes the resistivity at room temperature decrease rapidly, whereas the physical pressure reduces the resistivity increase at low temperatures. As a result, the doping system (x = 0.58) transforms from the semiconducting to the metallic one down to 90 K, and the resistivity for β'-$ET_3(ZnCl_4)_2$ under 12.6 kbar is almost constant down to low temperature.

(d) By doping ($GaCl_4^-$) to β'-$ET_3(ZnCl_4^{2-})_2$ with 1/2- filled band [2], the obtained β'-$ET_3(ZnCl_4^{2-})_{2-x}(GaCl_4^-)_x$ [x = 0.58] shows the metallic behavior down to 90 K. These systematic studies of band filling control suggest that the doping to 1/2-filled band is most effective.

References

[1] H. Mori, T. Okano, M. Kamiya, M. Haemori, H. Suzuki, S. Tanaka, Y. Nishio, K. Kajita, and H. Moriyama, *Physica C*, **357-360**, 103(2001).

[2] R. P. Shibaeva, R. M. Lobkovskaya, V. E. Korotkov, N. D. Kuahxh, E. B. Yagubskii, M. K. Makova, *Synth. Metals*, **27**, A457(1988).

Principal Publication and Authors

H.Mori, M. Kamiya[a,b], M. Haemori[a,b], H.Suzuki[a,b], S. Tanaka[a], Y.Nishio[b], K.Kajita[b], and H. Moriyama[b]

J. Am. Chem. Soc., **124**, 1251-1260(2002).

[a]ISTEC, [b]University of Toho

Theory of the Verwey Transition in Magnetite Fe_3O_4

H . Fukuyama

The transition metal oxide Fe_3O_4, called the magnetite, is a magnet that the human being has known from the early days. A modern scientific interest of this compound lies in the metal-insulator transition called the Verwey transition. Verwey has discovered this transition in 1939 [1], as a sudden jump in the resistivity at 120 K. In spite of numerous experimental as well as theoretical studies after the discovery, its origin remains to be clarified. The scenario of the charge ordering among the Fe ions at the B-sites, from a state with an average valence of +2.5 in the metallic state to an ordered state of +2 and +3 in the insulating state, has been believed as a most probable candidate, but its spatial pattern has not been uniquely identified up to now. Such a charge ordering phenomena attract interest in general, since they appear in many other systems, not only in the transition metal oxides, but also in organic conductors, rare earth compounds, and even in quantum hall systems.

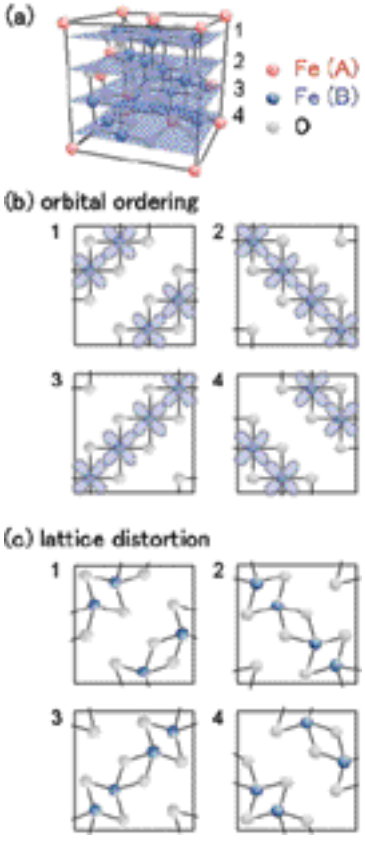

Fig. 1. Orbital order and lattice distortion proposed to be realized in magnetite Fe_3O_4. The spinel structure is shown in (a), where the A site Fe ions, the B site Fe ions, and the oxygen ions are represented by red, blue and white spheres, respectively. The ferro-type orbital order (b) and the bond dimerization (c), which we propose to be the origin of the insulating behavior in magnetite, is shown schematically in sectional views of the planes 1 ~ 4 shown in (a).

Recently, several experimental groups [2] have claimed that the charge ordering does not actually exist in the insulating state of magnetite. Motivated by these studies, we have proposed a mechanism of the Verwey transition in magnetite other than charge ordering based on the studies on the effects of the orbital degrees of freedom in the *d*-electrons of Fe ions, which has been recognized to play an important role in the presence of the strong Coulomb interaction, i.e., in the strongly correlated electron systems.

The Verwey transition is associated with the Fe ions at the so-called B sites of the spinel structure, shown in Fig. 1 (a). Their average valence of +2.5 at room temperature corresponds to half electron per site. We have investigated a 3-band spinless fermion model, which is known as a valid effective model for the Verwey transition in magnetite, since the spins are fully polarized ferromagnetically in the B sites due to the ferrimagnetic Neel order below 800 K. There, the electrons enter in the t_{2g} orbital which is triply degenerate due to the octahedral surrounding of the oxygen ions. In this case a charge ordereng can be realized due to the strong inter-orbital Coulomb interaction. It is important to note that this orbital order results in an effectively one-dimensional electronic structure as shown in Fig. 1 (b), characteristic of the spinel structure.

Such one-dimensionality of the electronic state is known to possibly result in the Peierls transition triggered by the electron-phonon interaction. The detailed studies show that it is actually possible, even in the three-dimensional structure of magnetite, if one considers the orbital degree of freedom. The lattice distortion accompanying this Peierls transition is schematically shown in Fig. 1 (c), where one can see that pairs of B sites are formed, which we call “bond dimerization”. Then the system becomes insulating without any charge ordering. This scenario is consistent with the existing experimental results and may give the solution to the “mystery” of the Verwey transition in magnetite.

References

[1] E. J. W. Verwey, Nature (London) **144**, 327 (1939).

[2] P. Novak, H. Stepankova, J. Englich, J. Kohout, and V. A. M. Brabers, Phys. Rev. B **61**, 1256 (2000); J. Garcia, G. Subias, M. G. Proietti, J. Blasco, H. Renevier, J. L. Hodeau, and Y. Joly, Phys. Rev. B 63, 054110 (2000); S. Todo, N. Takeshita, T. Kanehara, T. Mori and N. Môri, J. Appl. Phys. **89**, 7347 (2001).

Principle Publication and Authors

H. Seo[a], M. Ogata[b], and H. Fukuyama: *Aspects of the Verwey transition in magnetite*: Phys. Rev. B **65**, 085107 (2002).

[a]CERC, AIST Tsukuba, [b]Department of Physics, University of Tokyo

Interference Effect in Magnetic Circular Dichroism of Resonant X-Ray Emission Spectroscopy

A. Kotani

Resonant X-ray emission spectroscopy (RXES) has

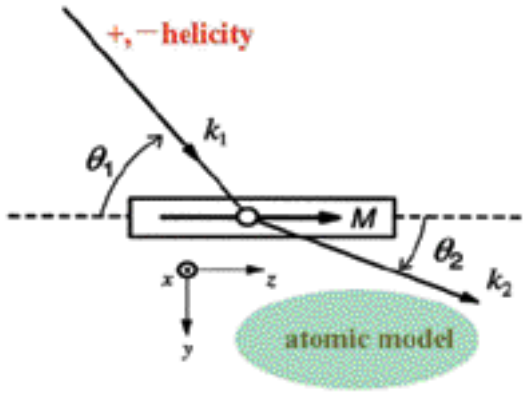

Fig. 1. Geometrical alignment of MCD in RXES is shown in the scattering plane. The θ_1 (θ_2) denotes the angle between the direction of incident (emitted) X-ray and that of the magnetization **M**. The MCD in RXES is a difference of RXES spectra for incident photons with + and – helicities, where the helicity of the emitted photon is not detected.

recently been a subject of remarkable progress due to the advent of high-brilliance synchrotron radiation sources. RXES is a photon-in and photon-out process, which is represented theoretically by a coherent second-order optical formula. [1]. The formula includes, in general, both real and virtual processes. In the real process, RXES consists of two successive processes, X-ray absorption from a ground state to a core-excited state and X-ray emission from this intermediate state to a final state. In the virtual process, on the other hand, two channels from the ground state to the final state via different intermediate states interfere each other, so that this is called *interference process*. Until very recently, the role of the interference process in RXES was not well understood, but very recently we have revealed theoretically that the interference process plays an essential role in magnetic circular dichroism (MCD) of RXES in a special geometry for ferromagnetic materials [2], and this finding has been confirmed by experimental observations [2].

Let us consider the situation shown in Figure 1. The magnetization of a thin-film is parallel to the sample surface and the angle between the incident X-ray (emitted X-ray) and the magnetization is θ_1 (θ_2) . The MCD in RXES (referred to as MCD-RXES) is defined by the difference of RXES spectra for incident photons with + and - helicities, where the helicity of the emitted photon is not analyzed.

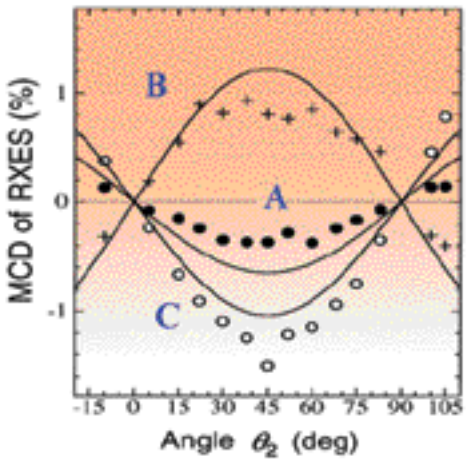

Fig. 2. Experimental result of θ_2 dependence of MCD-RXES in the transverse geometry for three different emitted photon energies A (closed circle), B (cross) and C (open circle). The solid curves are the calculated ones.

Within the atomic model, we have calculated the dependence of MCD-RXES on θ_1 and θ_2 . By group theoretical consideration, we have obtained a quite general analytic expression, and the result shows the following remarkable facts: The intensity of the real process is proportional to cos θ_1, while that of the interference process to sin θ_1. Therefore, when the incident X-ray direction is parallel to the magnetization (denoted by the longitudinal geometry), we have the 100 % real process contribution to MCD-RXES spectrum, while for the incident X-ray perpendicular to the magnetization (denoted by the transverse geometry) we have the 100 % interference process contribution. This result is surprising, because the interference effect in RXES is often considered to be negligibly small. Another remarkable point of the calculated result is that the θ_2 dependence of MCD-RXES intensity in the transverse geometry is proportional to sin $2\theta_2$.

Experimental observations of MCD-RXES spectra for longitudinal and transverse geometries have been made by Iwazumi *et al.* for the Gd $2p_{3/2}$-5d excitation and the 3d-$2p_{3/2}$ de-excitation of ferromagnetic Gd-Co amorphous alloy. The observed results are in good agreement with the calculated ones both in the spectral shape and the spectral intensity ratio in the longitudinal and transverse geometries. Furthermore, the θ_2 dependence of MCD-RXES spectra in the transverse geometry has also been measured and compared with the calculated result. The result is shown in Figure 2, where A(●) , B(+) and C(○) are intensities of a MCD-RXES peak by the $3d_{3/2}$-$2p_{3/2}$ transition, and of two MCD-RXES peaks by the $3d_{5/2}$-$2p_{3/2}$ transition, respectively, and they are displayed as a function of the angle θ_2. The theoretical result (sin $2\theta_2$) is also shown with the solid curves, and is found to be in reasonable agreement with the experimental result. This is the evidence that almost pure interference process has been observed in MCD-RXES experiments in the transverse geometry.

We would like to thank Dr. Iwazumi and his collaborators for their fine experiments.

References

[1] A. Kotani and S. Shin, Rev. Mod. Phys. **73**, 203 (2001).
[2] K. Fukui, H. Ogasawara, A. Kotani, T. Iwazumi, H. Shoji and T. Nakamura, J. Phys. Soc. Jpn. **70**, 3457 (2001).

Authors

A. Kotani, H. Ogasawara and K. Fukui[a]
[a]RIKEN/SPring-8

Lifting of Degeneracy of the Spin-1 Pyrochlore Antiferromagnets

K. Ueda

Since the pioneering work by Anderson [1] on the classical spin system with a disordered ground state, geometrically frustrated spin systems have been a fascinating subject. The pyrochlore lattice which is the network of the corner sharing tetrahedrons (see Fig.1) is the typical three dimensional frustrated system. This structure is found in a number of compounds including spinels, pyrochlores and C15-type Laves phase. For the spin-1/2 antiferromagnetic Heisenberg model, the quantum spin-liquid ground state is proposed based on the series expansion [2], but concerning the low-lying spin-singlet states below the spin gap a consistent picture has not emerged yet.

For spin-1 Heisenberg antiferromagnets, in contrast to

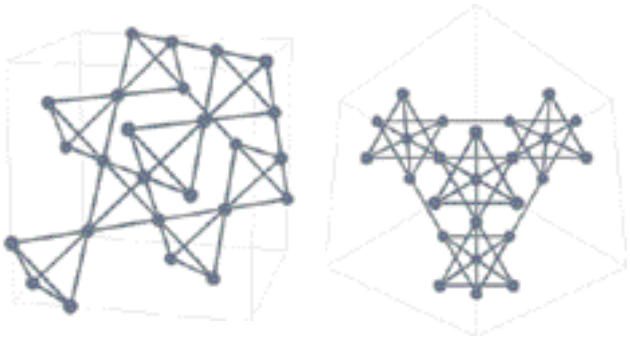

Fig.1. The primitive cell of the pyrochlore lattice (left panel) and its projected view from the origin to [111] direction (right).

the spin-1/2 cases, numerical methods are not powerful enough to draw definitive results and we need some analytic approach to solve the problem. Recently we proposed the idea of the tetrahedron-unit decomposition of the pyrochlore lattice [3], which is a natural generalization of the valence-bond-solid(VBS) state approach developed for the one-dimensional spin-1 antiferromagnets [4]. In this approach the ground states of the fundamental unit are the tetrahedron spin singlets which form the two-dimensional E representation of the tetrahedral group (T_d). Because of this degeneracy, the constructed variational wave functions for the ground state manifold have a macroscopic degeneracy.

Therefore, for the physics of the spin-1 pyrochlore antiferromagnets, it is essential to understand how the degeneracy is lifted. In principle, this degeneracy may be lifted within the model itself without introducing additional couplings. However, physically relevant ways of lifting may be through the couplings with other degrees of freedom. One plausible scenario is through the coupling with the local lattice distortion belonging to the same irreducible representation E: spin-driven Jahn-teller effect [3]. Actually the structural transition observed in some spinel compounds is consistent with this picture. Another relevant coupling may be the interactions between the tetrahedrons next to each other. For this case, the effective interaction can be mapped to an effective Hamiltonian of XY model, leading to a parity-broken ground state.

References

[1] P.W. Anderson: Phys. Rev. **102**, 1008 (1956).
[2] B. Canals and C. Lacroix: Phys. Rev. B **61**, 1149 (2000).
[3] Y. Yamashita and K. Ueda: Phys. Rev. Lett. **85**, 4960 (2000).
[4] I. Affleck, T. Kennedy, E.H. Lieb, and H. Tasaki: Phys. Rev. Lett. **59**, 799 (1987).
[5]Y. Yamashita, K. Ueda, and M. Sigrist: J. Phys.:Condens. Matter **13**, L691 (2001).

Authors

Y. Yamashita, K. Ueda and M. Sigrist[a]
[a]Theoretische Physik, ETH Zurich (Switzerland)

Quantum Melting of Charge and Spin Orders

M. Imada

Regular alignments of charge and/or spin densities of electrons are universally observable phenomena in electronic systems. These include charge (spin) density waves, charge orders including stripes, and antiferromagnetic (spiral) orders. A common feature in these phenomena is spontaneous breaking of the translational symmetry, where the

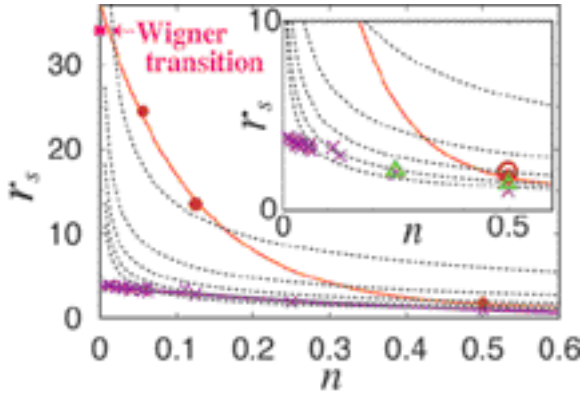

Fig. 1. Solid-liquid phase boundary in plane of the filling $n = 1/l$ with integer l and electron gas parameter r_s defined by the ratio of electron mean distance and the Bohr radius. The square indicates the Wigner transition point in the continuum limit. The path-integral renormalization group results (filled and open red circles for spinless and spin-1/2 fermions, respectively) are compared with the Hartree-Fock results (purple crosses for spinless and green triangles for spin-1/2 electrons). The red solid curves are guides for the eye. The dotted curves show contour lines for the ratio of the dielectric constant and the effective mass scaled by the bare values being at 1, 2, 3, 4 and 5 from up to down. The inset enlarges small r_s region. When the electron filling is changed with condition $n = 1/l$, and with fixed ratio of the dielectric constant and the effective mass, the system follows a contour line. With increasing l, the system undergoes a phase transition from a charge ordered insulator to a metal when crossing the red curve. Namely, the charge order undergoes a quantum melting when the fractional number of the commensurability becomes complicated. The Hartree-Fock calculation does not reproduce this trend of the quantum melting.

main origin of the periodicity formation is in many cases ascribed to electron-electron Coulomb interaction. In particular, the periodic alignment of charge and spin becomes remarkably stable if the electron concentration satisfies "commensurability condition", where the electron filling, n (namely, the number of conduction electrons in a unit cell) is a simple fractional number or integer. The Mott insulator is the most conspicuous example of such commensurate insulators, where the filling is an odd integer. Other many examples are found in charge orders of transition metal compounds and organic systems, where the filling is a simple fractional number such as 1/2 and 2/3. It is known that various dramatic and unsolved phenomena such as cuprate high-T_c superconductivity and colossal magnetoresistance in manganese oxides are observed closed to and under the proximity of such commensurate orders. For clarification of the mechanisms of such dramatic phenomena, it clearly requires elucidating mechanisms of commensurate insulator formation and its quantum melting. However, the stability of spin/charge orders only at some simple commensurate fillings is not well understood, which also means that the process of the quantum melting of these orders remains an open question.

We have studied the physics of quantum melting transitions of charge and spins. It has turned out that these transitions can indeed be successfully described only when taking account full quantum mechanical fluctuations beyond the mean-field level. For this purpose, we have developed new numerical as well as analytical tools, since the available tools have various types of difficulties in attacking them. The minus sign problem is known to be one of such difficulties, because of which, for example, most of numerical methods are not feasible for analysis of geometrically frustrated systems. The effects of frustrations have crucial importance in clarifying the quantum meltings as we see below. We have developed the path-integral renormalization

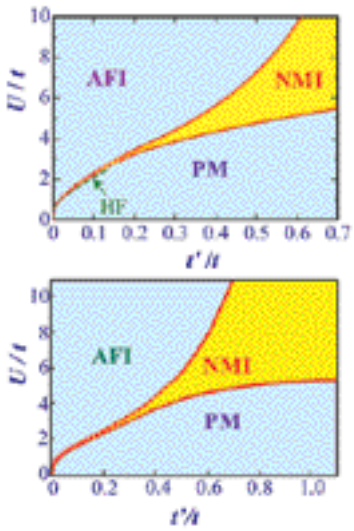

Fig.2. Phase diagram of the Hubbard model at half filling in the plane of the onsite Coulomb interaction scaled by the electron transfer U/t and the degree of the frustration t'/t for two choices of different lattice structures, namely the square lattice with next-nearest neighbor transfer (top panel) and anisotropic triangular lattice (bottom panel). AFI,NMI and PM represent AF insulator, nonmagnetic insulator, and paramagnetic metal, respectively. Green dashed curve in the upper panel shows the Hartree-Fock results for the metal-insulator phase boundary[8].

group method for numerical calculations [1,2] and the correlator projection method [3,4] for analytic treatments and have overcome the difficulties. In the path-integral renormalization group calculations, metal-insulator transitions, magnetic transitions and other possibilities of transitions are carefully examined with finite size scalings and extrapolations to the thermodynamic limit. With the newly developed tools, we have obtained the following remarkable insight.

(1) The charge order is indeed stabilized only at commensurate fillings with some simple fractions such as 1, 1/2, 1/3, 2/3, …, while quantum fluctuations destroy the ordering at other fillings [5]. For example, at n = 1/4, the charge order is stable at two-orders of magnitude larger electron density than the quantum melting point of the Wigner crystal in a 2D electron system in the continuum space (Figure 1). When the fraction k/l (with k and l being irreducible integers) becomes complicated with large l, the charge order quantum mechanically melts depending on the ratio of the effective mass and the dielectric constant. The Hartree-Fock calculation fails in accounting for such quantum melting and more elaborate calculations such as our method are crucial. Although the band theory predicts a simple distinction between metals and insulators, the real structure with long-range Coulomb interaction becomes much richer and more complicated than the band theory, because the simple metal a la the band theory actually has a rich and complex hierarchy structure with commensurate insulator phases contained.

(2) The spin orders in commensurate charge ordered state melt quantum mechanically when the geometrical frustration effects get large [6,7]. Quantum spin liquid phase then appears in a wide area adjacent to the metal-insulator transition and sandwiched by the metal and the antiferromagnetic insulator phases (Figure 2). In this spin liquid insulator phase, none of translational symmetry breakings such as dimer, and (staggered) flux state are stabilized and it is likely that the phase is not adiabatically continued to the band insulator.

(3) The order of metal-insulator transitions becomes from the first order to continuous when the geometrical frustration effects get large. This may be accounted for by the reduction of the spin correlations in the spin liquid phase. The reduction makes the interactions among the sites of holes and doubly occupied electrons (doublon) relatively small. This suppresses the phase segregation into the phase with rich doublons and holes, namely the liquid, and the phase with fewer doublons and holes, insulator. When the metal-insulator transition is the first-order type at zero temperature, it accompanies a first-order boundary line at finite temperature. This line starts at zero-temperature transition point and ends at a second-order critical point at a nonzero temperature. When the first-order transition is transformed to a continuous one at zero temperature, the accompanied first-order transition line at finite temperatures shrinks and its critical end point merges to zero temperature. Since the compressibility generally diverges at the critical end point, this causes the divergence of the compressibility at the zero-temperature metal-insulator transition point. Then the metal-insulator transition at zero temperature bears a marginal character between the first-order and continuous, since the compressibility divergence is the signal of the phase separation and the emergence of the first-order transition.

(4) Because of the compressibility divergence, the marginal character of the continuous metal-insulator transition alters the nature of the quantum critical phenomena (QCP) from the usual QCP expected with simple scaling laws to a more drastic one with structural formation, and self-organization, which is typical in complex systems. The divergence of the compressibility necessarily triggers the differentiation of electrons in the momentum space at the marginal point between localization and itinerancy. This yields sensitivity to external perturbations and serious competitions among instabilities to various orders such as superconductivity, charge/spin orders and ferromagnetism. Then these drastic effects now eventually accounts for the underlying physics of the high-T_c superconductivity and colossal magnetoresistance. This underlying physics is summarized by the emergence of extreme sensitivity of the systems to tiny perturbations such as magnetic fields and pressure as exemplified in the response in the colossal magnetoresistance. The same underlying physics generates coexisting instability to various orders as superconductivity and charge orders as well known in the high-T_c cuprates.

References
[1] M. Imada and T. Kashima: J. Phys. Soc. Jpn. **69** 2723-2726 (2000).
[2] T. Kashima and M. Imada: J. Phys. Soc. Jpn. **70** 2287-2299 (2001).
[3] S. Onoda and M. Imada: J. Phys. Soc. Jpn. **70** 632-635 (2001).
[4] S. Onoda and M. Imada: J. Phys. Soc. Jpn. **70** 3398-3418 (2001).
[5] Y. Noda and M. Imada: preprint (cond-mat/0203024).
[6] T. Kashima and M. Imada: J. Phys. Soc. Jpn. 70 3052-3067 (2001).
[7] H. Morita, S. Watanabe and M. Imada: preprint (condmat/0203020,J.Phys. Soc. Jpn. **71** NO9).
[8] W. Hofstetter and D. Vollhardt: Ann. Physik, **7** 48 (1998).

Author
M. Imada

GWΓ Method for the Self-Energy of a Many-Electron System

Y. Takada

In the last two decades, we have witnessed the power of quantum Monte Carlo (QMC) simulations that allow us to obtain virtually exact information on the static properties associated with the ground-state wave function of a quantum

many-body system. However, QMC cannot be used to evaluate dynamical properties, because dynamics requires information on excited-state wave functions as well. Thus we need to develop an alternative algorithm for dynamics.

Four decades ago, Baym and Kadanoff proposed a conserving approximation scheme by formulating the dynamical problem in terms of an energy functional $\Phi[G]$ with G the full Green's function. The self-energy Σ is obtained by $\Sigma = \delta \Phi[G] / \delta G$. One can choose $\Phi[G]$ at one's disposal. Although it is found to be very useful in many cases, this scheme never provides the exact Σ, because no algorithm is known to give exact $\Phi[G]$.

In 1995, I developed a conceptually new scheme to obtain the exact Σ, named the self-energy revision operator theory [1]; instead of pursuing $\Phi[G]$, I paid attention to the exact functional relations between Σ and the vertex function Γ, obeying the microscopic conservation law. In particular, Γ is determined through the Bethe-Salpeter equation with an irreducible electron-hole interaction given by the functional derivative, $\delta\Sigma/\delta\Gamma$. Starting from an arbitrary input, both Σ and Γ are iteratively revised towards self-consistency through the functional relations. Note that the number of terms representing Σ generated in this iterative process rapidly increases, eventually covering all terms derivable from the exact $\Phi[G]$ when the self-consistency is achieved.

In a numerical algorithm, however, the functional differentiation $\delta\Sigma/\delta\Gamma$ is not feasible, prompting me to invent an alternative scheme to revise G on a computer in an accurate and efficient way. Recently such a scheme is provided, giving an accurate enough result for Σ, in which the Ward identity is satisfied automatically [2,3]. This method allows us to obtain accurate results for the dynamical quantities, promising us to open a new dimension to the quantum many-body problems.

My calculation scheme is schematically shown in Figure 1, which indicates that this method may be regarded as an extension of the Hedin's GW method by including Γ that is determined self-consistently with Σ. Thus it is named the GWΓ method.

As an illustration, my method is implemented in the homogeneous electron gas at the density parameter $r_s = 4$ corresponding to sodium. The obtained single-electron spectral function $A(p,\omega)$ (which is given by $-\mathrm{Im}G(p,\omega)/\pi$) is shown in Figure 2. The main peak represents the structure of a quasiparticle. Its width is very sharp at and near the Fermi surface [Case (a)], indicating the existence of a well-defined quasiparticle. However, it is very broad far away from the Fermi surface [Case (b)]. In fact, its tail connects continuously with the plasmon-side band or the plasmaron (an entity composed of the real plasmon and the quasiparticle), implying a strongly decaying nature of the quasiparticle. Note that without Γ satisfying the Ward identity or the microscopic conservation law, this plasmaron peak does not come to the right energy position.

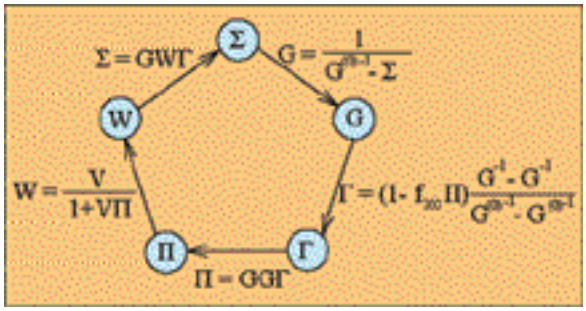

Fig 1. Schematic representation of my self-consistent calculation scheme for the self-energy Σ, where V is the bare Coulomb interaction, $G^{(0)}$ is the bare Green's function, π is the polarization function, and f_{xc} is the exchange-correlation kernel appearing in the time-dependent density functional theory.

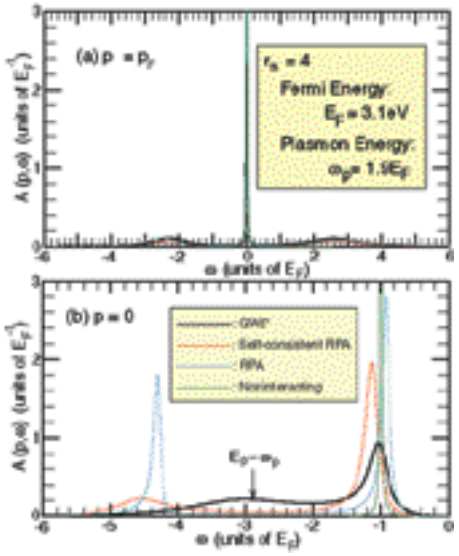

Fig 2. $A(p,\omega)$ for the homogeneous electron gas at the sodium density (a) at the Fermi surface ($p = p_F$) and (b) at the band bottom ($p = 0$).

My result of $A(p,\omega)$ discloses the intriguing complexity of the single-electron spectral function even in such a simple system as the electron gas, urging us to make a more detailed analysis of the experimental data obtained by angle-resolved photoemission spectroscopy (ARPES) in various materials widely ranging from simple to transition metals.

References
[1] Y. Takada, Phys. Rev. B **52**, 12708 (1995).
[2] Y. Takada, Int. J. Mod. Phys. B **15**, 2595 (2001).
[3] Y. Takada, Phys. Rev. Lett. **87**, 226402 (2001).

Author
Y. Takada

Spin-Triplet Superconductivity in Quasi-One Dimension

M. Kohmoto

In recent years the signs for unconventional superconductivity in many compounds have been accumulated. Examples include high superconductors, heavy fermions, organic conductors, Sr_2RuO_4, etc. The common features of those compounds are quasi-low dimensionality and proximity of antiferromagnetic (AF) order.

Here we consider seemingly the simplest quasi-one-dimensional systems which are realized in $(TMTSF)_2X$ family where X = PF_6, AsF_6, SbF_6, ClO_4, etc. (Bechgaard salts). At ambient pressure, most of these extremely anisotropic compounds undergo metal-insulator transition at low temperature and have a spin-density-wave(SDW) fundamental state. Under moderate pressure, the SDW instability is suppressed and replaced by a superconducting transition at a critical temperature of order of 1 K [1]. (One exception to this is $(TMTSF)_2ClO_4$ which is superconducting at ambient pressure.) Thus these compounds may be characterized by competition between superconducting and SDW ground states [2].

For the interaction, we consider AF magnetic coupling and weakly screened phonon-mediated interaction. In contrast to the previous works, we assume that the weakly screened phonon-mediated interaction is the driving force of superconductivity [3].
We also assume that AF fluctuation is not strong enough to give SDW gap. The spin-triplet superconductivity is possible because the Fermi surfaces are disconnected in quasi-one dimensional systems.

The weakly screened phonon-mediated interaction of spin-triplet pairing has the same magnitude as that of spin-singlet one. In many systems, however, only the spin-singlet superconductivity is realized. This is because the Fermi surfaces of usual matters are connected. In a system of connected Fermi surface, the requirement of parity and continuity does not admit the constant spin-triplet gap. Therefore, the s-wave superconductivity is favored from the kinematic reason. The quasi-one-dimensional system we consider, however, has disconnected Fermi surfaces, so it admits constant spin-triplet gap. Therefore, there is no reason to prefer s-wave superconductivity. In the case of constant gap, the interaction due to AF fluctuations act against the spin-singlet superconductivity more than the spin-triplet one, so the spin-triplet superconductivity is realized. This spin-triplet gap is nodeless.

To calculate the transition temperature T_c, we apply the BCS weak coupling theory. Since T_c of $(TMTSF)_2X$ is rather low, one can expect that the strong coupling corrections do not change our results qualitatively. For the sake of simplicity, the cutoffs of the phonon-mediated interaction and AF one are taken to be same and denoted by ω_D and the width of the peaks of these interactions are taken to be same as Γ. The open Fermi surface is given by $k_x=\pm c$ .We approximate the spin-singlet gap ψ by $\psi_{k_x=c} = \psi_{k_x=-c} = const$ and the spin-triplet gap $\vec{d}$ by $\vec{d}_{k_x=c} = -\vec{d}_{k_x=-c} = const$. If we denote the density of states on the Fermi surface as N_{k_F} and the strength of phonon interaction and AF interaction as f (0) and f (Q), the critical temperature of the spin-singlet superconductivity becomes

$$T_c^{even} = 1.13\hbar\omega_D e^{1/\{N_{k_F} V^{even}\Gamma^2/4\pi^2\}},$$

where $V^{even} = -f(0) + 3J(Q)$, and that of spin-triplet becomes

$$T_c^{odd} = 1.13\hbar\omega_D e^{1/\{N_{k_F} V^{odd}\Gamma^2/4\pi^2\}},$$

where $V^{odd} = -f(0) + 3J(Q)$ .From the above equations, the condition $T_c^{odd} \geq T_c^{even}$ is always satisfied in the present case. Thus $T_c^{odd} \geq T_c^{even}$ and spin-triplet superconductivity is present if $V^{odd} = -f(0) + J(Q) < 0$. This result shows that this superconductivity disappears if AF fluctuations dominate. On the other hand spin-triplet superconductivity is realized if phonon-mediated interaction dominates. Since $\vec{d}_k$ is an odd function, the gaps at the open Fermi surfaces $k_x=\pm c$ have opposite signs and there is no node in the gap.

References

[1] For a review, see T. Ishigro, K. Yamaji and G. Saito, Organic Superconductors (Spring-Verlag, Berlin) 1998.
[2] D. Jérome, A. Mazaud, M. Ribault and K. Bechgaard, J. Phys.(Paris) Lett., **41** L95 (1980) .
[3] M. Kohmoto and M. Sato, Europhys. Lett., **56** (5), 726-740 (2001).

Principal Publication and Authors

M. Kohmoto and M. Sato

Quantum Hall Systems under Lateral Modulation Potential

Y. Iye

The quantum Hall effect (QHE) system ---- two-dimensional electron gas (2DEG) subjected to a quantizing magnetic field ---- provides an experimental stage for ever fascinating physics. There are many different regimes of Landau level filling factor, ν , each of which involves characteristic length scales. Therefore, by imposing an external modulation potential with periodicity close to such length scales, one can perturb the QHE system in a non-trivial way, and hence extract useful piece of information, or even create new states.We have studied magnetotransport in 2DEG subjected to a short period (a = 92 nm) one-dimensional modulation potential as shown in Fig.1.

Geometrical resonance of composite fermions

The concept of composite fermions (CFs), first advanced by J.Jain and elaborated by many subsequent studies, one of the most successful models to describe some aspects of the quantum Hall systems in a pictorial way. One of the unsettled issues is the spin state of CFs. As for the ν = 1/2 CFs, it is established that they are fully spin polarized. For ν = 3/2, however, the existing data are somewhat contradictory.

Figure 2 shows the magnetoresistance trace for a modulated 2DEG sample, in comparison with a plain 2DEG. The former trace exhibits commensurability oscillation features near ν = 3/2, which arise from geometrical resonance of CF cyclotron radius with the modulation period. Detailed analyses of the positions of the resistance dips shown in Fig.3 indicate that the ν = 3/2 CFs are fully spin polarized.

Stripe phase in half-filled higher Landau levels

The fractional QHE and CF Fermi liquid behavior occur in the lowest Laudau levels (LLs). In higher LLs, the electronic ground states are quite different. Recently, anisotropic states are discovered at half-filled higher LLs in ultrahigh quality 2DEG samples with mobility in excess of 1000m^2/Vs. The anisotropic state is attributed to occurrence

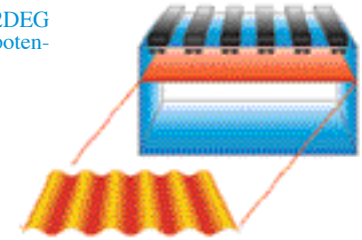

Fig. 1. GaAs/AlGaAs 2DEG sample with periodic potential modulation.

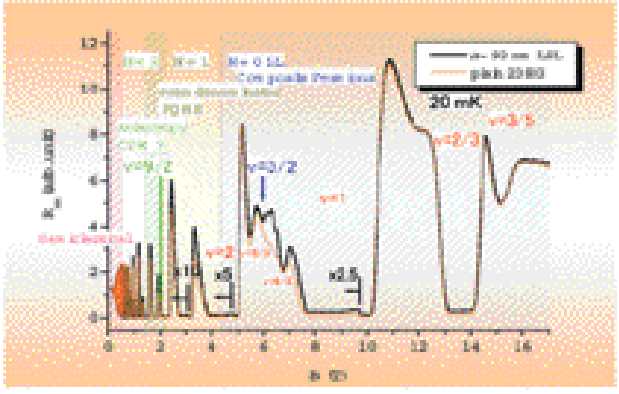

Fig.2. Magnetoresistance traces for a plain (red) and a modulated (black) 2DEG. The difference is most conspicuous around the filling ν = 3/2.

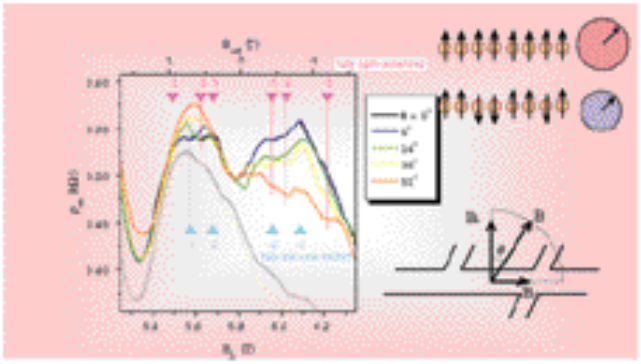

Fig.3. Expanded view of the traces near $\nu = 3/2$. The positions of the resistance dips are consistent with those predicted by assuming fully spin polarized CFs.

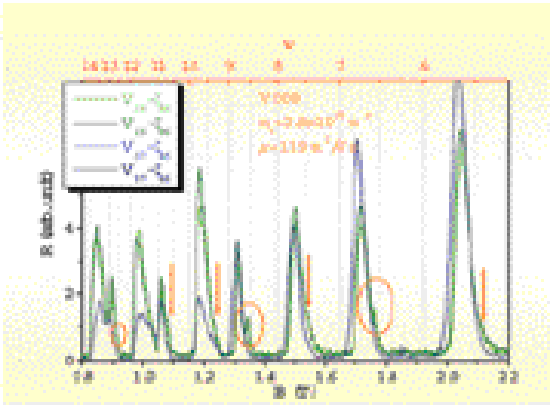

Fig.4 Magnetoresistance traces obtained for different current directions in a modulated 2DEG over the range, $5 < \nu < 14$. The features indicated by arrows and circles correspond to stripe phase at half filled higher Landau levels.

of stripe phase, or a kind of charge density wave state.

Although the mobility of our 2DEG samples is about 100 m^2/Vs, similar features have been observed in modulated samples as shown in Fig.4. This finding suggests that the stripe phase can be stabilized by external modulation potential of appropriate periodicity. We have found that such features at fillings as high as $\nu = 25/2$, and also at $\nu = 7/2$ and 5/2, for which the ground state of plain 2DEG is known to be an even denominator FQHE.

References

[1] A. Endo, M. Kawamura, S. Katsumoto and Y.Iye
Phys. Rev. B**63** 113310-1-4 (2001).

[2] A.Endo and Y.Iye
Solid State Commun. **117** 249-254 (2001).

Authors

A. Endo, S. Katsumoto, Y. Iye

Continuum Meets Discrete in an Aharonov-Bohm Interferometer

S. Katsumoto

An electron is a quantum, which is a particle and at the same time, a wave. The charge of single electron (namely the basic charge) was first measured by Millikan in 1911 (till 1913), by using tiny oil-droplets, which are maybe the first "quantum dots". In modern experiments such single-electron charging effect appears in so called "single-electron transistors", which are composed of electrodes and small

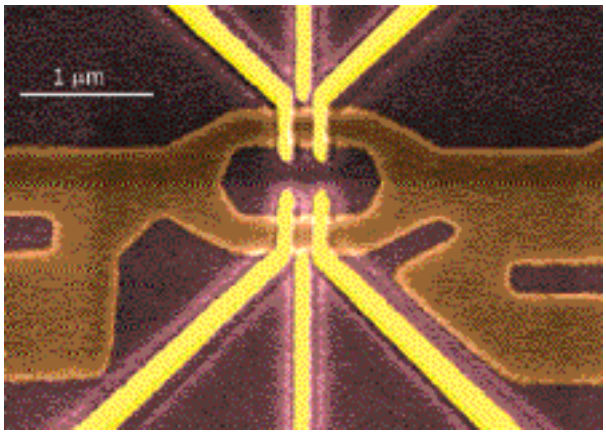

Fig.1. Scanning electron micrograph of the sample. The ring structure was fabricated by electron-beam lithography and wet-etching. The bright yellow regions indicate gate-electrodes made of Au. They are placed to constitute quantum dot (or single-electron transistor) on each path of the AB interferometer

metallic islands (quantum dots or Coulomb islands).

While the charging effect represents the particle-side of electrons, the interference effect reveals the other side, i.e., electrons as waves. The interference of two partial waves is determined by the phase difference, which can be tuned by the magnetic flux threaded inside the loop consists of their trajectories. This is a kind of Aharonov-Bohm effect, which is observable as an oscillation of electric conductance through metallic rings of mesoscopic size against external magnetic field.

Then a natural question is "what happens when a quantum dot is placed on a metallic loop, i.e., an Aharonov-Bohm (AB) interferometer?" Into the language of energy spectrum, this question is interpreted as "what happens when a system with discrete energy levels is embedded in the continuum?" A basic answer to the question was theoretically given by Fano in 1961 [1]. The two states merge into a new state (Fano resonant state), which sits in between the two extremes of a quantum.

The simplest natural realization of the above question is a single atom embedded in delocalized states. This results in characteristic asymmetric line-shapes of resonance peaks, which are widely observed in various physical systems and known as the Fano effect. However, these natural systems have little controllability and the examination beyond the line-shape has been an untouched issue. We have observed

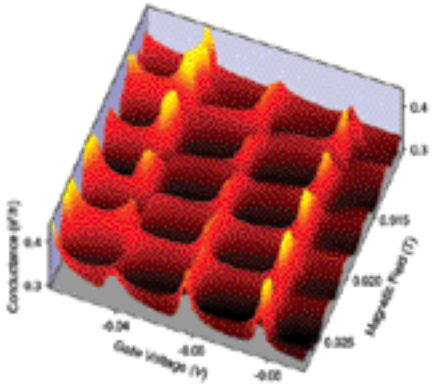

Fig.2. Conductance through an AB interferometer with a quantum dot in one of its arms. The two axes in plane are the external magnetic field and the gate voltage of the dot. The oscillation along the voltage is Coulomb oscillation and that along the magnetic field is AB oscillation. Note that the asymmetry in the Coulomb-line-shape changes its parity when the field passes the maxima of the AB oscillation.

and examined the Fano effect for the first time in an artificial quantum dot – AB ring hybrid system and obtained an essentially new insight that the Fano parameter which is the key variable in the effect should be complex number.

Figure 1 shows a scanning electron micrograph of the fabricated device. A two dimensional electron gas at a (Ga,Al)As/GaAs hetero-interface was mesa-etched into a small ring (AB interferometer) structure, and thin wires of Au were placed to form quantum dots interrupting the electron paths and to control the electro-static potential of them. The sample was cooled down to 30 mK and the magnetic field up to 7 T was applied.

Figure 2 displays the conductance through the ring as a function of the applied magnetic field and the gate voltage. For this measurement, the gate-voltages were adjusted to form a quantum dot in one arm and to open the other to form continuous a ring-interferometer. The oscillation versus the gate voltage is due to the discrete levels formed by single-electron charging effect and called "Coulomb oscillation". Unlike usual Coulomb oscillation, the line-shapes are asymmetric manifesting a Fano state are formed.

At the same time, an oscillation versus magnetic field is observed, which is the AB oscillation. Hence the system shows the both aspects of electrons as "quanta". What is remarkable here is the parity of the asymmetric line-shape changes when the magnetic field passes the maxima of the AB oscillation. The parity as well as detailed line-shape is determined by so called the "Fano parameter" q, which has been conventionally treated as a real variable. However the data shown in Fig.2 manifest that q is a function of at least two parameters. And the simplest way to treat the situation is to treat q as a complex variable. Further study to clarify the many-body effects on the Fano state is now under way.

References
[1] U. Fano, Phys. Rev. **124**, 1866 (1961).

Authors
K. Kobayashi, H. Aikawa, S. Katsumoto and Y. Iye

Correlated Motion of Small Ag Clusters and Ge Dimer-Bucklingon Ge(001) as a Precursor Process of Surface Alloying

F. Komori

The motion of atoms and small clusters at surfaces is an important subject not only for the fundamental understanding of the stability of material but also for the fabrication of novel and functional materials by such as alloying or chemical reactions. Still the dynamical processes prior to the alloying at surfaces have not been well studied.

Among various surface alloys and compounds, Ag on clean Ge(001) has attained a special interest since the discovery of superconductivity below 2 K.[1] This system is a candidate for the superconducting surface alloy because Ag and Ge are immiscible and not superconductors in the bulk. The growth of Ag on Ge(001) has been previously studied by scanning tunneling microscopy (STM) at room temperature (RT). [2] When sub-monolayer (ML) Ag is deposited on Ge(001) surfaces at 90 K, they form 1 ML thick two dimensional (2D) islands and one-dimensional (1D) chains after annealing at RT as shown in Fig. 1. The 2D island is stable at RT and the corrugation on the island is small in STM observations. This suggests that alloying occurs at the Ag-Ge interface during the annealing to RT.

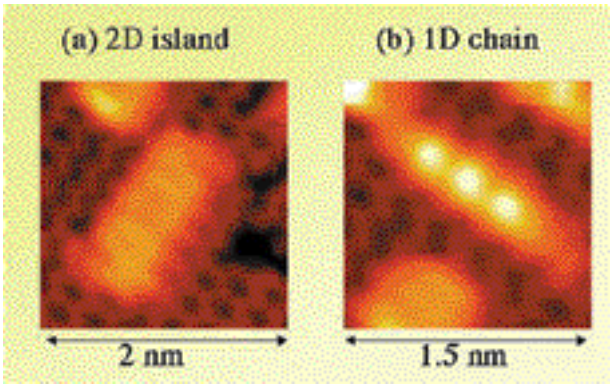

Fig. 1. STM images of 0.35 ML Ag deposited Ge(001) surface at 90 K, observed at 65 K after 13 hours annealing at RT. The 2D island (a) and the 1D chain (b) are formed on this surface. The former elongates along the Ge dimer row direction and occupies three dimer rows. The latter elongates along the Ge dimer direction and has mono-atomic width.

We have studied Ag on Ge(001) surfaces by STM at temperatures between 65 K and RT to understand the processes of Ag island formation and their intermixing into the Ge surface by increasing the temperature. Silver was always deposited at 90 K. The deposited Ag atoms or their small aggregates are randomly located at various sites on Ge(001) at 78 K, and are observed as small and large bright dots in the STM images. Some of the dots move on the surface with keeping the phase of the substrate Ge dimer buckling. By increasing the sample temperature, the bright dots diffuse, transform and assemble into small clusters, which are still one mono atomic layer thick. Finally, above 200 K, the clusters occupying three Ge dimer rows transform into the 2D islands with small corrugation. The images inside the 2D island and the 1D chain were found not to be the cluster types of the bright dots. This suggests Ag dots move on the surface and intermix or alloy with the substrate Ge atoms during the annealing.

On 0.2 ML Ag deposited Ge(001) after annealing at 180 K for 2 hours, we found the clusters made of the large dots

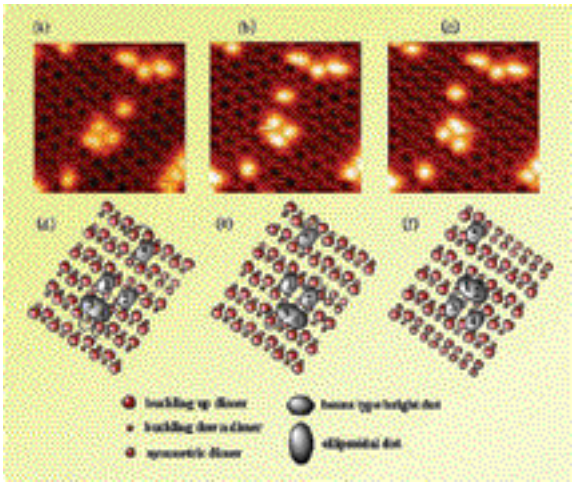

Fig. 2. (a-c) Successive STM images at 180 K with about 5 min interval including a cluster made of two kinds of the Ag dots on three Ge dimer rows.(d-f) Schematic diagram of the dots and the cluster motion in (a-c). In (a, d), two bright dots indicated by 1, 2 are located in the trough between Ge dimer rows, and an ellipsoidal dot, indicated as 3-4, is located in the lower left adjacent trough between the rows. Next in (b, e), the location of the ellipsoidal dot moves to the lower right side along the Ge dimer row. In the third (c, f), the locations of the two bright dots and an ellipsoidal dot are exchanged. The isolated large dot indicated by 5 in the figures also moves along the Ge dimer row.

as well as isolated large dots. Figures 2 show successive STM images with 5 min interval, and their models. As in the models, the thermally-activated motion of the Ag dots causes the buckling change of the Ge dimer and vice versa at this temperature. Especially, the movement of the bright dots along the dimer row in the cluster induces the simultaneous formation and separation of the ellipsoidal dots with correlated change of the buckling phase at the Ge dimer rows under the cluster. These correlated motions are precursor processes to the formation of the 2D alloy islands above 200 K.

References
[1] M.J. Burns, J.R. Lince, R.S. Williams and P.M. Chaikin, Solid State Commun. **51** 865 (1984).
[2] F. Komori, K. Kushida, K. Hattori, S. Arai and T. Iimori, Surf. Sci. **438** 123 (1999).

Authors
Y. Naitoh, K. Nakatsuji and F. Komori

Spectroscopic Evidence for Asymmetric Dimer of Si(100) at Very Low Temperature

J. Yoshinobu

Surface atoms on Si(100) are reconstructed to form a (2 × 1) dimer row structure [1]. Many experimental and theoretical studies have supported the buckled (asymmetric) dimer with c(4 × 2) phase as a ground state. However, recently, several low temperature STM studies have reported symmetric dimer images [2-5], and the origin of symmetric images is still controversial. In this study [6], using high resolution Si 2p photoelectron spectroscopy [7,8], we have investigated the electronic states of Si(100) at 140 K, 100 K and 55 K.

The experiments were performed in an ultrahigh vacuum (UHV) chamber, where the base pressure was 7 × 10^{-11} Torr. Boron-doped p-type Si(100) wafers (3~5 Ωcm) were used in the experiments. Clean Si(100) surfaces were prepared after being outgassed at ~ 900 K for 12 hours, flashed up to 1550 K several times, and cooled slowly from ~ 1000 K to 140 K, 100 K or 55 K. High resolution Si 2p PES measurements were performed at BL-16B with an undulator radiation source of Photon Factory in KEK. The photoelectrons were collected with a hemispherical analyzer. The total instrumental energy resolution of the present experiments was below 80 meV when the photon energy was 129 eV. It should be noted that in our LEED measurements sharp c(4 × 2) patterns were observed at 55 K, 100 K, and 140 K.

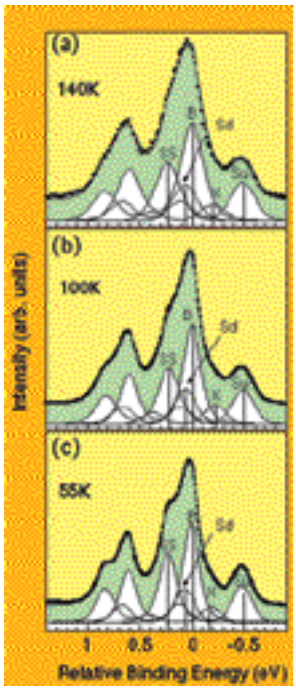

Fig. 1. Si 2p PES spectra for the Si(100) surface (a) at 140 K, (b) 100 K, (c) 55K. The emission angle was 0° and the photon energy was 129 eV.

Figure 1 shows the Si 2p PES spectra for the Si(100) surface at 140K, 100 K and 55K. By carefully analyzing the spectra and the plots of relative area intensity of each component as a function of emission angle, we can decompose the spectrum into five components and assign them [6-8]: the components B is due to the bulk Si atoms; the components Su and Sd correspond to the up and down Si atoms of the asymmetric dimers, respectively; the component SS is assigned to second layer Si atoms. The component X is still unidentified. The split of 550 meV between the up and down dimer components comes from a substantial charge transfer within the dimer atoms, indicating that the asymmetric dimers have some ionic character. The peak positions and the angle dependence of intensity ratios agree well with the previous results [7].With decreasing the temperature, the spectral shapes become sharper due to reduced thermal broadening, but the spectra at 140 K, 100 K, and 55 K are basically similar. Thus the local structure of Si(100) surface at 140 K, 100 K, and 55 K must be the same. The intensity ratio of the up and down dimer peaks are almost the same in this temperature range, indicating that the asymmetric dimer structure of Si(100) does not change between 55 K and 144 K. Thus, we conclude that the dimer on Si(100) is asymmetric down to 55 K, and the origin of symmetric images in STM is due to dynamic or extrinsic effects.

Table I. Summary of relative area intensities of each component at normal emission.

	Su	Sd	B	SS	X
140K	0.15	0.15	0.39	0.24	0.07
100K	0.15	0.15	0.38	0.24	0.08
55K	0.15	0.14	0.37	0.27	0.07

References
[1] R. E. Schlier and H. E. Farnsworth, J. Chem. Phys. 30, 917 (1959).
[2] H. Shigekawa *et al.* , JJAP part2 39, (1997) **L1081**, and JJAP par1 39 3811 (2000).
[3] T. Yokoyama and K. Takayanagi, Phys. Rev. B**61**, R5078 (2000).
[4] T. Mitsui and K. Takayanagi, Phys. Rev. B **62**, R16251 (2000).
[5] Y. Kondo et al, Surf. Sci. **453**, L318 (2000).
[6] Y. Yamashita, S. Machida, M. Nagao, S. Yamamoto, Y. Kakefuda, K. Mukai and J. Yoshinobu, Jpn. J. Appl. Phys. **41**, L272 (2002).
[7] E. Landemark et al, Phys. Rev. Lett.**69**, 1588 (1992).
[8] E. Pehlke and M. Scheffler, Phys. Rev. Lett. **71**, 2338 (1993).

Authors
Y. Yamashita, S. Machida, M. Nagao, S. Yamamoto, Y. Kakefuda, K. Mukai and J. Yoshinobu

Magnetoresistance in Fractional-Layer Oxide Superlattices

M. Lippmaa

Transition metal oxides are well known for the wide variety of interesting and useful physical properties. Our work is aimed at understanding the growth process of oxide thin films and the properties of oxide surfaces and interfaces.We mainly concentrate on the perovskite-type materials that have similar structures and lattice constants. This similarity leads to the possibility of artificially constructing lattices in thin film form. Crystal growth by pulsed laser deposition (PLD) is possible even when the growth conditions are far from thermodynamic equilibrium. It is thus feasible to build lattices which can not be grown in bulk form.

An example structure of an artificial material is shown in Figure 1. This particular structure, also known as a fractional layer superlattice or an epitaxial nanocomposite, consists of a matrix material, shown in red, and nanodots (blue), which are embedded at regular intervals in the matrix. We have selected a ferromagnetic metallic oxide, $La_{0.6}Sr_{0.4}MnO_3$ for the matrix layers and $La_{0.6}Sr_{0.4}FeO_3$, which is antiferromagnetic in bulk form, for the nanodots.

As shown in the model image in Figure 1(a), the ferromagnetic order, and thus also metallic conductivity, is lost in the matrix layers immediately surrounding the nanodots, forming insulating bubbles in the lattice. The size of such bubbles is reduced when an external magnetic field is applied (Figure 1(b)) due to the partial restoration of metallic conductivity in the atomic layers which are not in direct contact with the nanodots. If the nanodot density is carefully adjusted, it is possible to grow a thin film which is close to a percolative metal to insulator transition [1]. Without an external field the nonconducting bubbles touch, and the lattice is insulating. When an external field is applied, the bubbles shrink and conduction paths open (Figure 1(b)).

This behavior can be seen in the resistivity vs. temperature plots measured at various magnetic fields, as shown in Figure 2. The largest magnetoresistance effect was achieved in a lattice containing nanodots with an average diameter of 25 nm at a coverage of 0.5 monolayers. The nanodot layers were separated from each other by three layers of the matrix material. As shown in the plot, the material is an insulator when no field is applied. Metallic behavior, i.e. drop of resistivity with decreasing temperature, appears when an external magnetic field of 1 Tesla or more is applied.

When nanodots with a smaller diameter are used, such as 5 nm, conduction paths do not form even in a field of 7 Tesla. The magnetoresistance behavior of the constituent

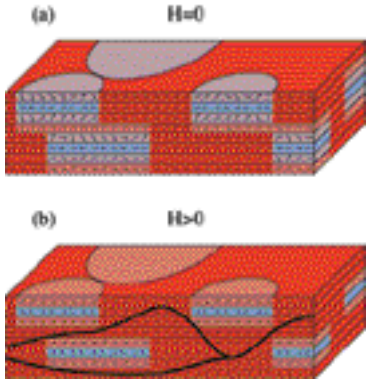

Fig. 1. A cross section of a fractional layer superlattice consisting of a ferromagnetic and metallic matrix (red) and embedded nanodots (blue). Each nanodot has a thickness of just 0.4 nm, i.e. a single unit cell. Regions of reduced conductivity, which surround the nanodots, become smaller when an external field is applied, opening conduction paths.

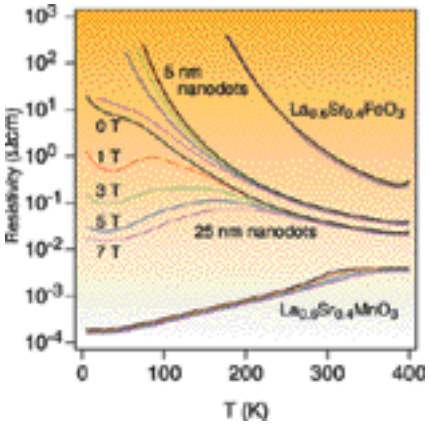

Fig. 2. Magnetoresistance in fractional layer superlattices. The average nanodot diameter in the two samples was 25 nm and 5 nm. Temperature behaviors of the two component materials are also shown for comparison.

materials, $La_{0.6}Sr_{0.4}MnO_3$ and $La_{0.6}Sr_{0.4}FeO_3$, are also shown for comparison. Fractional layer superlattices offer a new way of creating thin film materials with properties that can be tuned by changing the shape, size, or density of the nanostructures used. Due to the local nature of interactions that determine the bulk transport properties, these superlattices can also be used for studying the electronic structure of oxide heterointerfaces in general. It is particularly important to distinguish between various competing mechanisms which are present close to the interface, such as exchange interactions, cation diffusion, and charge transfer.

References

[1] N. Nakagawa, M. Lippmaa, K. Shibuya, H. Koinuma, and M. Kawasaki, Jpn. J. Appl. Phys. **41**, L302 (2002).

Authors

M. Lippmaa, N. Nakagawa[a], K. Terai and K. Shibuya

[a]Bell Laboratories (USA)

Generation and Application of the World Highest Magnetic Fields

N. Miura

At the Megagauss Laboratory (MGL) of ISSP, two techniques have been so far developed to generate very high magnetic fields in the megagauss range (>100 T). They are the single-turn coil technique and electromagnetic flux compression. The former technique is useful for handy experiments in the 100-200 T range, as the samples are preserved intact in each shot in spite of the violent destruction of the coil. Electromagnetic flux compression, on the other hand, is a powerful technique for even higher magnetic fields. By compressing the magnetic flux with an imploding metal ring (liner) driven by a large pulsed primary current through a one-turn coil (primary coil), we can generate a field exceeding 500 T.

Recently, we have developed a new device called “feed gap compensator” by which we improved the symmetry of the liner deformation resulting in a considerable increase of the maximum available field. One of the serious problems which restricted the maximum field was the existence of the “feed gap” in the primary coil. This causes an asymmetric liner deformation, and the protrude towards the feed gap induces a generation of plasma jet which often destroys the sample before the maximum field is reached. By employing

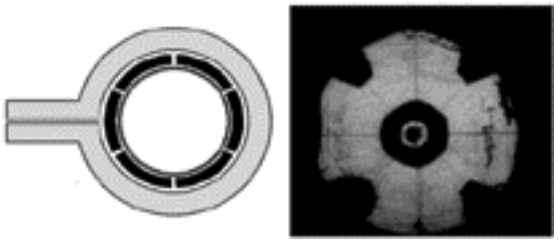

Fig. 1. (Left) Sketch of a primary coil and a liner for electromagnetic flux compression with a feed gap compensator in between. When we supply a large pulsed current of the order of 5 MA to the primary coil, a secondary current is induced in the liner in the opposite direction, and the repulsive force between the two currents rapidly squeezes the liner. This motion of the liner towards the inward direction compresses the magnetic flux inside which has been injected beforehand. 6 pieces of Cu blocks that are inserted between the primary coil and the liner being electrically insulated are the feed gap compensator. Without the compensator, the magnetic field near the feed gap is always weaker than the other part, and this causes an asymmetric deformation of the liner. With the compensator, the symmetry was much improved.
(Right) High speed photograph of the imploding liner (shadow graph). Reflecting the 6 slits in the compensator, the deformed liner has a hexagonal symmetry. The deformation without the compensator is very different, involving a protrude and the shift of the center of gravity towards the feed gap.

the feed gap compensator as shown in Fig. 1, we found that the liner symmetry was much improved. As a result, we succeeded in generating a magnetic field up to 622 T. Figure 2 shows the waveforms of the magnetic field and the primary current when we obtained 622 T. This is the highest magnetic field which has ever been produced by indoor experiments in the world.

Such a high magnetic field is an extremely powerful experimental tool for investigating solid state physics, since it will drastically alter electronic states in solids. We can expect that it will open up a new area of physics beyond the existing theory. In fact, we have found many new phenomena in a variety of materials under the extremely high magnetic fields [1-3]. As an example, we show in Fig. 3 the magneto-optical spectra in a GaAs/AlAs quantum well in a magnetic field above 500 T. The data show the exciton line and many absorption lines due to the inter-Landau level transitions. A number of new features are observed in the

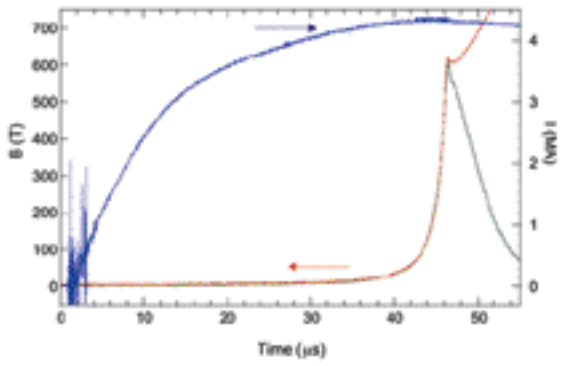

Fig. 2 Waveforms of the primary current *I* and the magnetic field *B*, generated by electromagnetic flux compression. The signals from 2 pick up coils are shown for *B* (red and green curves). The 2 graphs coincide almost precisely until the pick up coils are destroyed at about 46 μs. showing the accuracy of the field measurement. Just before the destruction of the coils, the turn-around effect (the field starts decreasing after taking the maximum) is seen in the both curves.

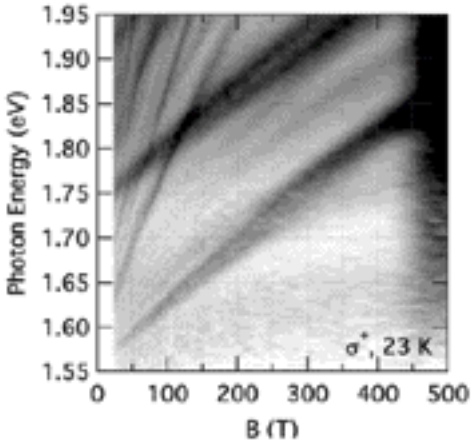

Fig. 3. Magneto-absorption spectra in GaAs/AlAs quantum wells. The thickness of the layers is 9.0 nm and 5.0 nm for GaAs and AlAs, respectively. The temperature was 23 K. The line at the lowest photon energy is due to the exciton absorption. The exciton line shows a discontinuity at about 240 T. This field corresponds to the magnetic field at which the wave-function extension along the magnetic field is reduced to the thickness of the layers of GaAs. The study of excitons in very high magnetic field is of interest in connection with the fundamental problem of physics concerning hydrogen atoms in extremely high magnetic fields such as those existing in neutron stars (~10^8 T). Although the field available in our experiments today is several orders of magnitude less, its effect on excitons is comparable with that the field in neutron stars gives on hydrogen atoms due to the large dielectric constant and the small effective mass of the material.

spectra, such as the broadening, discontinuity, sudden emergence and disappearance of the absorption lines.

References

[1] T. Hayashi, N. Miura, K. Noda, H. Kuwahara, S. Okamoto, S. Ishihara and S. Maekawa: Phys. Rev. B **65** 024408 (2002).
[2] Y. H. Matsuda, T. Ikaida, N. Miura, S. Kuroda, F. Takano and K. Takita: Phys. Rev. B **65** 115202 (2002).
[3] N. Miura, H. Nakagawa, T. Sekitani, M. Naito, H. Sato and Y. Enomoto: to be published in Physica B **319** (2002) 310.

Principal Publication and Authors

N. Miura, Y. H. Matsuda, K. Uchida, S. Ikeda and F. Herlach: Proceedings of the 4th International Conferences on the Physical Phenomena in High Magnetic Fields (Santa Fe, 2001). (World Scientific, 2002) P.513.

Development of Advanced Experimental Techniques under Pulsed Ultra-High Magnetic Fields

T. Osada

We have developed two novel experimental techniques for use in pulsed high magnetic fields at the megagauss laboratory (*MGL*) of *ISSP*. One is the direct magnetotransport measurement under pulsed ultra high magnetic fields up to 600 T using RF bias and PSD technique. The other is the high sensitivity torque-meter under 50 T-class pulsed magnetic fields with use of a micro-cantilever.

Ultra-high magnetic fields exceeding 100 T can be obtained only as a single-shot pulse using destructive methods. At *MGL*, ultra-high magnetic fields are generated by use of two types of methods. One is the single-turn coil method generating the maximum field of 200 T, and the other is the electromagnetic flux compression method generating the maximum field of 620 T, which is the world record of the in-house high magnetic fields. However, their effective pulse width is so short (several μsec) that experiments

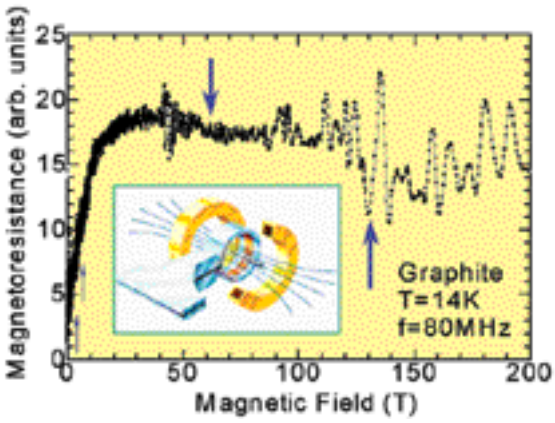

Fig. 1. Magnetoresistance of single crystal graphite under pulsed ultra-high magnetic fields generated by the electromagnetic flux compression device (inset). Large arrows indicate the new Shubnikov-de Haas structures.

are very difficult because of huge discharge noise, huge induced voltage, and self-heating of samples.

In order to overcome these difficulties, we have employed RF bias (f = 30~100 MHz) and phase sensitive detection (PSD) technique. Temperature increase due to self-heating can be suppressed by decreasing sample size. The magnetoresistance of single-crystal graphite and quasi-two dimensional organic conductor α-(BEDT-TTF)$_2$KHg(SCN)$_4$ was successfully measured under vertical magnetic fields up to 200 T generated by the flux-compression method. In graphite, new Shubnikov-de Haas oscillations were observed at unexpected positions in high magnetic fields. This result suggests the importance of correlation effects in graphite in ultra-high magnetic field region.

The other technique is the high sensitivity micro-scale magnetic torque measurement. A high-sensitive miniature torque-meter is developed with use of a commercial piezo-resistive micro-cantilever for atomic force microscope (AFM). A sample mounted at the end of a cantilever beam produces magnetic torque $\tau = M \times B$ in a magnetic field, and the resultant deflection of the beam is detected electrically. Resistance through a piezo-resistive path is precisely measured with a Wheatstone bridge circuit. This makes it possible to detect a small change in magnetization of samples of less than 1 mg, and the sensitivity is evaluated as the order of m ~10^{-13} Am^2 at 40 T, which is superior to conventional induction methods. The micro-cantilever technique has been applied to the oxide superconductor Sr_2RuO_4, organic conductor α-(BEDT-TTF)$_2$KHg(SCN)$_4$, *etc*.

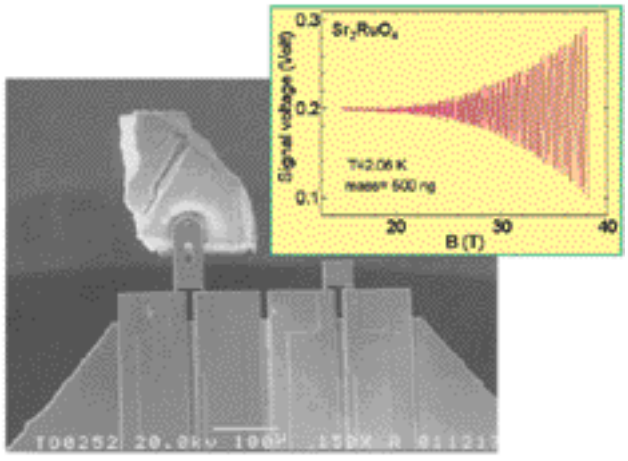

Fig. 2. Scanning electron microscope image of the micro-cantilever on which a small sample crystal is mounted. Inset: de Haas-van Alphen oscillations measured in Sr_2RuO_4.

Principal Publication and Authors

T. Osada, E. Ohmichi, S. Ikeda, M. Kuraguchi, T. Inokuchi, K. Kobayashi, M. Saito and M. Kobayakawa

Maturity of Non Magnetic 4GPa Class High Pressure Cell

Y. Uwatoko

Undoubtedly, the study of the physical properties at high pressure, high magnetic field and low temperature is one of the important subjects for the understanding of highly correlated electron systems, in which the various attractive phenomena such as superconductivity and magnetically ordered non-Fermi liquid have been induced under pressure. Until now, many scientists have designed a nonmagnetic piston cylinder type high pressure cell made of nonmagnetic Cu-Be alloy [1]. Unfortunately, the pressure limit should be only up to 20 kbar due to the limit of the tensile strength of Cu-Be alloy. Recently, however, the new high pressure cells made of Ni-Cr-Al alloy (Russian alloy) and Co-Ni-Cr-Mo alloy (MP35N) have been tested successfully up to a pressure of 31.5 kbar and 35 kbar, respectively. These strong non-magnetic materials Ni-Cr-Al and MP35N have been introduced by Eremets *et al*. [2] and Walker [3]. In the field of the solid state physics at low temperature the mechanical and magnetic properties of Ni-Cr-Al alloy seems to be better than those MP35N alloy.

For optimum mechanical properties which were obtained at aging condition of 700℃ for 2 hours, the hardness became about 57 HRC.

The alloy showed the ultimate tensile strengths of over 2 GPa, which is almost similar to that of MP35N alloy [3], and the true strain of about 2 %.

We have analyzed the magnetic properties of a sample of a heat-treated Ni-Cr-Al alloy, MP35N and Cu-Be alloy by SQUID magnetometer (Quantum Design). The magnetic susceptibility of Ni-Cr-Al alloy is almost ten times lager than that of Cu-Be alloy. The Ni-Cr-Al shows no temperature dependence in susceptibility, while the MP35N has

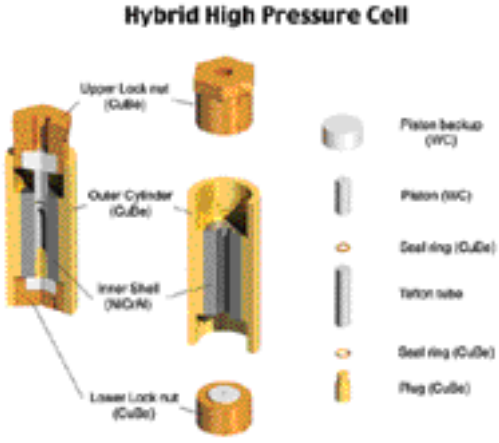

Fig. 1. Design of 4GPa Class Non Magnetic High Pressure Cell. The dimensions of inner NiCrAl cylinder are 25, 14 and 5 mm, in length, outer diameter and inner diameter. Basic idea of cell is similar to the former designed hybrid cells [2,3]. The high pressure sample space was sealed by Teflon cell technique. As a pressure transmitting fluid

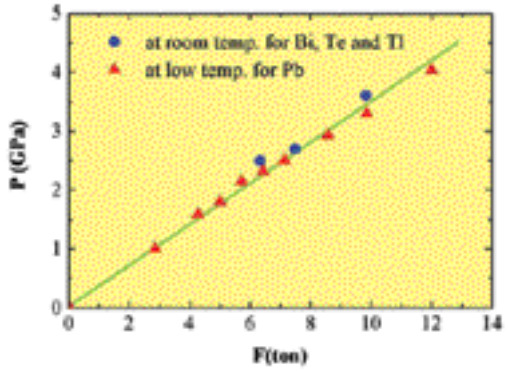

Fig. 2. Pressure versus applied force. There is one linear variation at room and low temperature up to 4 GPa.

large temperature dependence. In this respect the Ni-Cr-Al is conclusively better material for high pressure cell at high magnetic field and low temperature. These materials are not ferromagnetic at least down to 2 K.

We have designed a conventional piston cylinder cell, which consists of a nonmagnetic WC and the Ni-Cr-Al inner cylinder inserted into the Cu-Be outer sleeve. A schematic drawing of the pressure cell is shown in Fig. 1.

The pressure at room temperature and liquid helium temperature were determined from P-T phase diagram for Bi, Tl, and Te and the superconducting transition temperature $T_C(P)$ for Pb, which have well known pressure dependence. From the data measured in this study, at room and low temperatures pressure is shown as a function of applied force in Fig. 2. There is one linear variation at room and low temperature up to 4GPa. As a final results, it has been found that a maximum working pressure could be raised constantly up to P = 4 GPa at T = 30 mK without any trouble.

References

[1] H. Fujwara, H. Kadomatsu and K. Tohma: Rev. Sci. Instrum. **51**, 1345 (1980).
[2] M. Eremets: High Pressure Experimental Methods, Oxford University Press 1996.
[3] I.R. Walker: Rev. Sci. Instrum. **70**, 3402 (1999).

Authors

M. Hedo, S. Todo, Y. Uwatoko, M. Kosaka[a], N. Mori[a] and T. Matsumoto[b].
[a]Department of Physics, Saitama University, Urawa 338-8570, Japan
[b]National Institute for Materials Science, Tsukuba 305-0047, Japan

Positive Ion Mobility in Normal Liquid ^{3}He under High Magnetic Fields

H. Ishimoto

The ion in liquid ^{3}He is a powerful tool not only for studying elementally excitations but also for understanding the behavior of heavy charged particle in neutral Fermi liquid. The positive ion called " snowball " is a cluster of ^{3}He atoms attracted to the core $(^3He)_2^+$ by its large local electric field. Existence of the localized ^{3}He spins on the ion surface makes the positive ion a sort of magnetic impurity which is intentionally produced in extremely pure Fermi liquid. The radius is the order of 1 nm, which grows with an applied liquid pressure. At low temperatures below 100 mK, the ion interacts with Landau quasi-particles, and hence the situation resembles a Kondo effect in metal. However in liquid ^{3}He, the ionic recoil is important because of the absence of lattice. Although the inelastic energy exchange is considered to explain a Log ($1/T$) dependence of positive ion mobility below 100 mK, the magnetic exchange scattering between the ion and the quasi-particles could be relevant to it. To clarify the scattering mechanism, the positive ion mobility has been measured under higher magnetic fields up to 15 T at various pressures and temperatures.

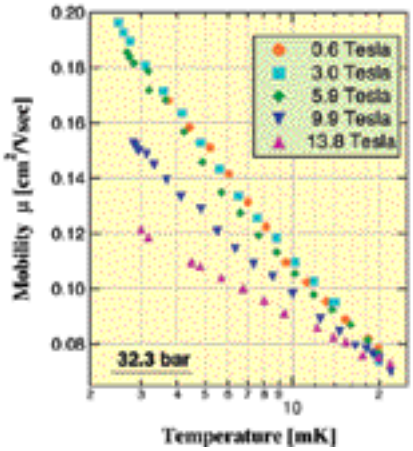

Fig.1. Temperature dependence of the positive ion mobility at 32 bar for various magnetic fields. The slope of the Log ($1/T$) dependence

The temperature dependence of the mobility at P = 32 bar is given for various magnetic fields in Fig.1. Below 20 mK, the Log ($1/T$) dependence does exist even at high magnetic fields up to 14.8 T. The magnetic field dependence at constant temperature is more surprising. The mobility exhibits a small broad peak followed by a large decrease at 3.2 mK. The behavior is seriously affected by the liquid pressure as shown in Fig.2. The peak shifts to the high field side with decreasing the pressure, and is followed by a large decrease above 25 bar. On the other hand no magnetic field dependence is observed for the negative ion called " electron bubble " in the same pressure and temperature region. Therefore the field dependence in the positive ion mobility is attributable to the magnetic interaction between the ^{3}He quasi-particles and the localized spins on the ion surface.

What is a microscopic mechanism? Variation of the bulk

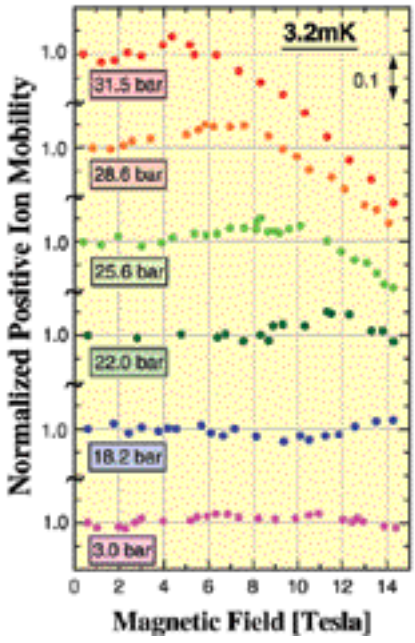

Fig.2. Magnetic field dependence of the positive ion mobility at 3.2 mK for various pressures.

liquid ^{3}He properties and the melting pressure with magnetic field is not large enough to explain it. The other possible origin could be the localized ^{3}He spins on the snowball, which causes a large magnetization under high magnetic field. It should suppress a spin flip exchange scattering of the quasi-particles, resulting into the increase of the mobility. At the same time, it induces a polarized spin density arising from the RKKY spin oscillation in the vicinity of the snowball, leading the enhancement of the scattering cross section and hence the decrease of the mobility. A delicate competition between these two factors seems to cause a complicated field dependence of the mobility. To understand clearly the scattering of the snowball under high magnetic fields, a new theoretical treatment is eagerly desired.

Principal Publication and Authors
K. Obara, D. Ueno, V. Efimov, R. Masutomi, A.Yamaguchi and H. Ishimoto, Phys. Rev. Lett. **87** 235301 (2001) .

THz-Electron Spin Resonance in a Big-Bang

H. Nojiri and N. Miura

THz-electron spin resonance is a unique method to investigate magnetic as well as electronic property of solid. THz-regime is a new developing field of spectroscopy and it is useful to investigate a strong spin-phonon coupling in low dimensional magnets and strongly correlated electron systems.

Since a resonance field exceeds 100 T, a use of non-destructive field generator is necessary for such experiments. A very short interval of a field pulse as well as a noisy environment have prevented a realization of such experiment. Use of a high power far-infrared laser and an advanced shielding system have enabled us to perform THz-electron spin resonance in mega-gauss fields. Very clean spectrua can be observed at low temperatures as shown in Fig. 1.

As the first experiment, a spin-phonon coupled mode in $CuGeO_3$ is observed. A splitting of the mode in low field has been interpreted as the change of incommensurate lattice distortion in the magnetic phase. The present result shows how the incommensurate wave vector changes in the very middle (the saturation field is about 250 T) of the magnetic phase where no other microscopic spin probe can access.

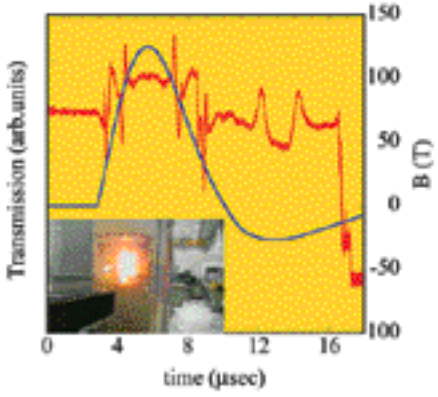

Fig. 1. Example of ESR spectrum (red) in FeF_2 at 25 K with a freguency $\nu = 2.52$ THz and a field trac e (blue). Inset shows a photograph at the instance of field generation. In the big explosion of a single-turn coil, a very clean signal is obtained and the sample can be recovered undestroyed.

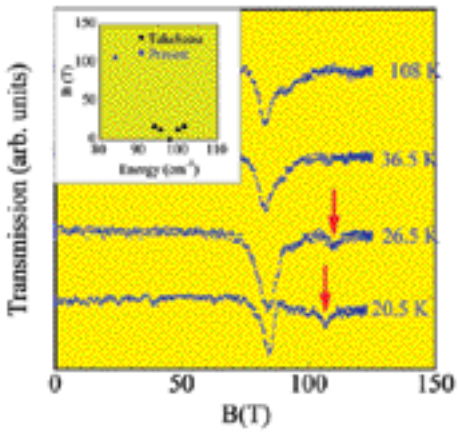

Fig. 2. A spin-phonon coupled mode of $CuGeO_3$ (red arrows) is observed at 107 T in the middle of incommensurate magnetic phase. The strong-polarization dependence indicates that the mode is not a pure spin resonance mode. Field dependence the mode is analyzed in connection with previous data taken at low fields [1].

Reference
1)K. Takehana *et al*., J. Phys. Soc. Jpn., **70** 3391 (2001).

Authors
H. Nojiri[a] , Y. H. Matsuda and N. Miura

Dynamical Study on Room-Temperature Huge Magnetoresistance Effect

H. Akinaga and N. Miura

[a]Department of Physics, Okayama University

There has been increasing interest in magnetoresistance (MR) effect with a view to its application in various magnetic devices, such as a magnetic field sensor. The spin-dependent MR effect in artificial structures, such as metallic multilayers and tunnel junctions, have attracted much attention, raising scientific and technological issues. Rapid increase in the recording density of hard disk drives requires the continuous development of the magneto-electronics devices.

Recently, we developed successfully new MR materials consisting of nanoscale metal islands that are grown on a GaAs substrate [1]. The material shows more than thousand-

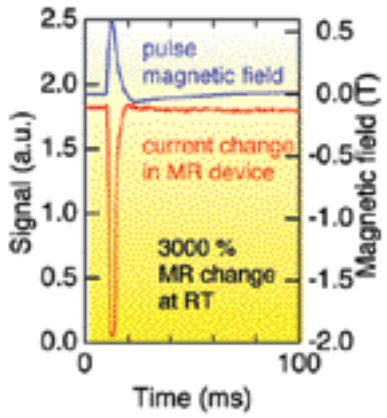

Fig. 1. The current evolution as a function of time, under an influence of the pulsed magnetic field. The MR ratio calculated from the current change reaches more than 3000 %.

fold MR change under a relatively low magnetic field, even at room-temperature (RT). The new MR material shows the highest magnetic-field sensitivity compared with the existent MR materials and devices in the magnetic-field range of a few hundred Oe. We termed the new phenomenon Magnetoresistive switch. In the fiscal year of 2001, we have investigated the dynamics of the magnetoresistive switch effect. The magnetic-field sensitivity and the response time of the effect are decisive parameters for the sensor application. As a result of the investigation, we have found a method to improve the dynam-ic properties of the new MR material [2].

This work was partly supported by the New Energy and Industrial Technology Development Organization (NEDO).

References

[1] H. Akinaga, M. Mizuguchi, K. Ono and M. Oshima, Appl. Phys. Lett. **76**, 357-9 (2000).
[2] H. Akinaga, N. Miura and K. Uchida, Patent pending.

Authors

H. Akinaga[a], K. Uchida, Y. Matsuda and N. Miura
[a]Research Consortium for Synthetic Nano-Function Materials Project (SYNAF), National Institute of Advanced Industrial Science and Technology (AIST)

Measurement of the Intensity-Dependent Atomic Dipole Phase of a High Harmonic by Frequency-Resolved Optical Gating (FROG)

S. Watanabe

High harmonics generated by nonlinear interaction between the intense laser field and atoms are of great interest for the potential application to science and technology in vacuum ultraviolet (VUV), extreme ultraviolet (XUV) and soft x-ray regions. Recently, theoretical analyses and experiments in the strong field approximation reveal that high harmonic pulses have an intensity-dependent phase, i.e. atomic dipole phase, inducing negative chirp in a high harmonic pulse [1]. Thus, appropriate phase compensation compresses the high harmonic pulses to the attosecond regime. However, the phase of a high harmonic pulse has never been measured so far. One of the techniques commonly used for charactering the ultrashort pulses fully is frequency-resolved optical gating (FROG) [2], involving the measurement of the time-dependent spectrum of the autocorrelation or cross-correlation (spectrogram) and the solution of the pulse retrieval problem mathematically. In this work, we have developed two-photon-ionization (TPI) FROG and measured the temporal profile, including the phase, of the fifth harmonic of Ti:sapphire laser for the first time, from which the negative chirp of a high harmonic was confirmed.

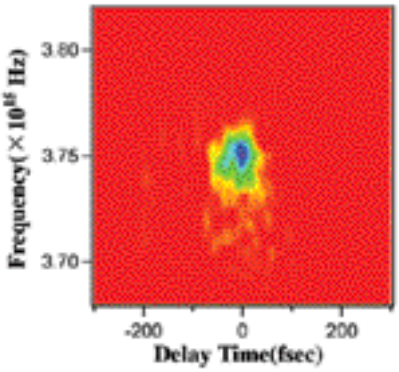

Fig. 1 TPI photoelectron spectrogram of the fifth harmonic of Ti : sapphire laser.

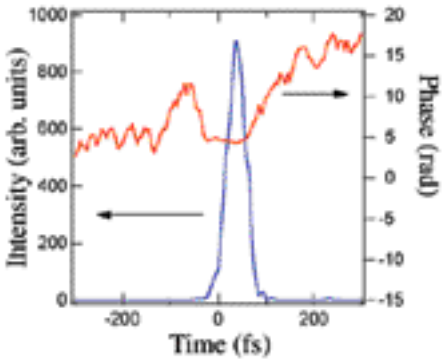

Fig. 2. Retrieved pulse shape and phase of the fifth harmonic of Ti:sapphire laser after a 2-mm thick CaF_2 plate. The phase is constant within the pulse duration, indicating that the pulse is almost Fourier-transform limited.

Figures 1 and 2 show the spectrogram constructed from the time-dependent TPI photoelectron spectra and retrieved pulse profile of the fifth harmonic of Ti:sapphire laser after a 2-mm thick CaF_2 plate, respectively. The temporal duration of the pulse was 50 fs. The phase shown in Fig. 2 is almost flat within the pulse duration, indicating that the pulse is almost Fourier-transform limited. Because TPI is the second order process, a TPI spectrogram is symmetric with respect to time reversal and the temporal direction cannot be determined by one spectrogram. Thus, the thickness of the CaF_2 plate, i.e. phase dispersion, was changed to 0.5 or 4 mm and the pulse profiles were measured. The temporal direction was determined to be consistent among the retrieved pulses, taking account of the phase dispersion. The changes in the pulse profiles are explained well, confirming that TPI FROG measurement is valid. From these results, the temporal shape just after the generation of the harmonic pulse was calculated and the pulse was found to have negative chirp. The amount of the chirp agrees with the estimation by a theoretical model in the strong field approximation. This work supports the theoretical description of high harmonic generation and suggests the attosecond pulse generation by appropriate phase compensation. By using a shorter laser pulse and generating higher harmonics, attosecond pulses will be obtained, revealing unprecedented phenomena, such as electronic motions in materials.

References

[1] M. Lewenstein, P. Salières, and A. L'Huillier, Phys. Rev. A **52**, 4747 (1995).
[2] R. Trebino, *et al.*, Rev. Sci. Instrum. **68**, 3277 (1997).

Principal Publication and Authors

T. Sekikawa, T. Katsura, S. Miura, and S. Watanabe
Physical Review Lett **88**, 193902 (2002).

Direct Phase Measurement of the X-Ray Specular Reflection Using Modulation under the Bragg Condition

T. Takahashi

Specular reflectivity of X-rays, giving information on the electron density distribution perpendicular to the surface, is a helpful method in studying the structure of surfaces,

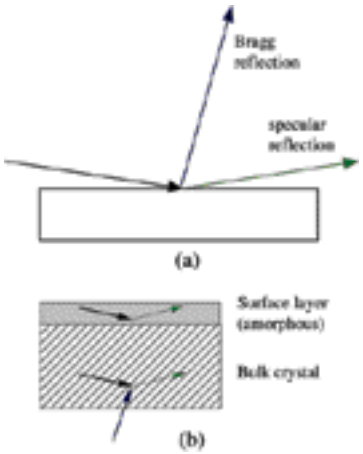

Fig.1. Illustration of experimental condition where specular reflection is measured when a Bragg reflection is excited (a). When the surface layer has no periodicity in the direction parallel to the surface or has a periodicity different from that of the substrate crystal, the specular reflection of the surface layer is excited only by the incident wave while that of the bulk is excited both by the incident and diffracted waves (b).

interfaces, and thin films. However, as is the case in X-ray intensity measurements, one is faced with the so-called phase problem due to lack of phase information on reflected waves through the detection of X-rays as intensities. For this reason one must construct a number of structural models until a model explains experimental results well. Nevertheless, one can directly get a structural model from experimental results if one could obtain phase information from the experimental results.

In the structure analysis of 3D crystals, such studies getting phase information have been made extensively. In contrast, in the structural analysis of surface layers only a few studies have been done. In this report we show a new method to obtain directly the phase of X-ray specular reflection using its intensity modulation by exciting a Bragg reflection on the substrate crystal, particularly useful for surface layers without the same lateral periodicity as the substrate crystal. Figure1 shows a basic idea of the present work. When a Bragg diffraction condition except the symmetric Bragg diffraction is satisfied by the substrate crystal, the Bragg diffracted wave is excited only in the substrate crystal as illustrated in Fig.1 (b). In this situation, specular reflectivity is given as a sum of three components, A_0 (substrate) +A_h (substrate) +A_0 (surface). Since the structure of the substrate crystal is known, the amplitudes of the incident wave A_0 (substrate) and the diffracted wave A_h (substrate) are known. When the substrate is a nearly perfect

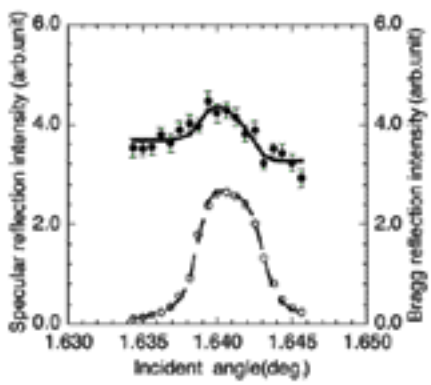

Fig.2. Intensity changes of X-rays as a function of incident angle of X-rays. Filled and open circles respectively correspond to the intensities of specular reflection and 113 Bragg reflection.

crystal such as silicon, the phase of the diffracted wave A_h (substrate) changes as a function of incident angle around the Bragg angle according to the dynamical theory [1]. Thus the measurement of intensity modulations of specular reflectivity under the diffraction condition gives information of the amplitude and the phase of specular reflected wave by the surface layer, A_0 (surface).

We applied the method to a Si(001) single-crystal whose surface was covered with a layer of native oxide a few nanometers thick, that is considered to be amorphous in its structure [2]. Figure 2 shows an experimental result of X-ray intensities as a function of incident angle. From the intensity modulation of specular reflection indicated by filled circles, the phase and the amplitude of A_0 (surface) were determined to be 6.36x10^-3 and 0.26x2π, respectively. It should be noted that the absolute value of the modulus of A_0 (surface) is obtained without measuring absolute reflectivities.

This result indicates that in principle one can determine the structure of the surface layer by the Fourier transform of a set of A_0 (surface)'s if one repeats such measurements by scanning the wavelength of the incident wave to vary the perpendicular momentum transfer of specular reflection. A preliminary result supporting the present method has been obtained, which will be described elsewhere.

References
[1] T. Takahashi and S. Nakatani, Surf. Sci. **326** 347 (1995).
[2] W. Yashiro, K. Sumitani, K. Hirano, T. Takahashi, Jpn. J. Appl. Phys. **41** L592 (2002).

Authors
T. Takahashi, W. Yashiro, K. Sumitani and K. Hirano[a]

Nonmagnetic-Impurity-Induced Antiferromagnetic Long-Range Order in Quantum-Disordered Antiferromagnets

H. Takayama

[a]Photon Factory, KEK

In low dimensional antiferromagnets, such as a bond-alternating antiferromagnetic (AF) chain, or a 2 dimensional (2D) antiferromagnet consisting of bond-alternating AF chains coupled with AF interchain interactions, a pair of spins coupled with a stronger interaction forms a singlet and so their ground state is non-magnetic and associates with a finite excitation energy, the so-called spin gap. Here we call them quantum-disordered antiferromagnets. We have determined the ground-state phase diagram of the 2D antiferromagnet above-mentioned in the parameter space of the strengths of bond-alternation and interchain coupling by means of the quantum Monte Carlo simulation with the continuous-imaginary-time loop algorithm (CITLA-QMC).

Our interest of the present work is to reveal what happens on the nonmagnetic, spin-gapped ground state when non-magnetic impurities are introduced. We have considered two effects of the latter; one is site dilution, i.e., a non-magnetic atom is substituted for a magnetic atom, and the other is bond dilution, i.e., a non-magnetic atom breaks an exchange interaction between spins.

Site-dilution effect

For the site dilution, it is natural for us to imagine the following scenario. Since the spin system of our present

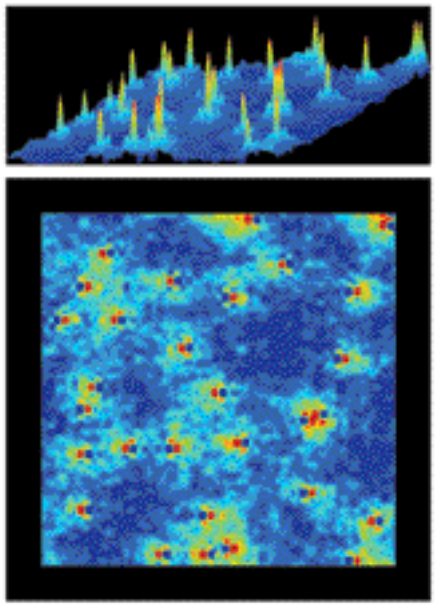

Fig.1 Real-space distribution of magnetic moments in the ground state of a site-diluted 2D AF Heisenberg model consisting of bond-alternating (-J-J'-J-J'-) AF chains coupled with AF interchain interactions J". The values of the parameters are J=1, J'=J"=0.5, and 30 diluted sites on a 64×64 lattice. The upper (lower) figure is the 3D (2D) representation. The magnetic moments are peaked at sites connected by a strong bond with diluted sites. Each of them has a significant spatial extent whose size is the AF coherence length of the medium, i.e., the sea of singlets.

interest is not frustrated, a spin which loses its partner of a singlet by dilution behaves as an almost free (or classical) spin. Between these free spins the residual interactions exist through paths connecting them. The interactions are exponentially small as a function of the distance between two free spins, but they keep the staggeredness with respect to the original lattice since the dilution does not induce frustrations. Consequently, in the ground state the AF long-range order (AF-LRO) carried on these free spins is expected even with an infinitesimal concentration of dilution.

By the CITLA-QMC simulation we have thoroughly justified the above-mentioned scenario, which we call that of the dilution-induced AF-LRO on a sea of singlets [1]. In Fig. 1 the real-space distribution of magnetic moments is shown. The AF-LRO is ascertained by examining the staggered spin correlation function. The staggered magnetization

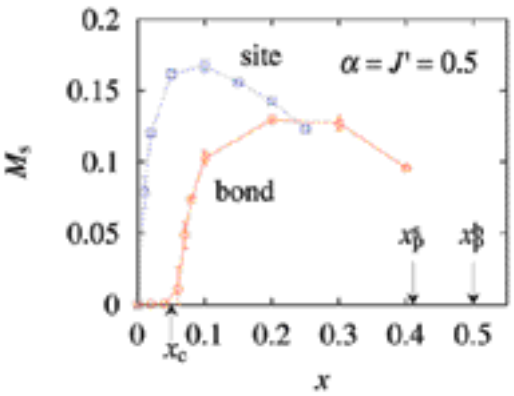

Fig.2 Concentration dependences of the staggered magnetization M_s in the site- and bond-diluted systems with J = 1 and J' = J" = 0.5. There exists the critical concentration x_c of about 0.05 in the bond-diluted system. The arrows with x_p's indicate the percolation thresholds on the site and bond dilution problems, at which M_s is expected to vanish.

depends on the concentration of dilution as shown in Fig. 2, from which we conclude the critical concentration x_c above which the AF-LRO appears is zero.

Bond-dilution effect

We may think that the above scenario of the AF-LRO on a sea of singlets can be applied also to the bond-dilution case if we take into account one difference that there appear two, instead of one, free spins at both ends of a diluted strong bond. However this is not the case, since these two spins are coupled antiferromagnetically by interaction J_{af} via the shortest paths which are proportional to JJ"J". If the strength of J_{af} is larger than that of the effective interactions between free spins at different strong bonds diluted, Jeff, which is certainly the case for a small concentration of dilution, the two spins reform a singlet by J_{af}. Thus the critical concentration x_c is expected to be finite for the bond-diluted system in contrast to $x_c = 0$ for the site-diluted system.

The staggered magnetization data obtained by the CITLA-QMC simulation [2] and shown in Fig. 2 clearly indicate the existence of a finite critical concentration x_c for the bond-dilution case. We have also confirmed a new spin gap proportional to J_{af} within the original spin gap of the non-diluted system. A further interesting phenomenon coming out from the competition between J_{eff} and J_{af} is a possible existence of the quantum Griffiths phase. Our data strongly suggest that the spin gap vanishes at concentration $x_{c'}$ which is smaller than x_c. Detailed simulations to specify the properties of the phase between $x_{c'}$ and x_c are now in progress.

References
[1] C. Yasuda, S. Todo, M. Matsumoto, and H. Takayama, Phys. Rev. B **64** 092405 (2001).
[2] C. Yasuda, S. Todo, M. Matsumoto, and H. Takayama, Prog. Theor. Phys. Suppl. **145** 399 (2002).

Discovery of Missing Link: II. A Spin-1/2 Pyroxene Compound $NaTiSi_2O_6$

A.N. Vasil'ev and Y. Ueda

Authors
C. Yasuda , S. Toda , M. Matsumoto and H. Takayama

The alkali metal pyroxene family denoted as $AM^{3+}B_2O_6$ (A = alkali metal; B = Si, Ge) was previously studied from a mineralogical standpoint. The compound $NaAlSi_2O_6$ named jadeite or "hisui" in Japanese and $LiAlSi_2O_6$ called "kunzite" after the mineralogist Dr. G. F. Kunz have been very precious stones since ancient times. Recently, the pyroxene compounds with transition metal ions M^{3+} have drawn great attention as one-dimensional (1D) magnets. In the crystal structure of pyroxene (Figure 1), the $M^{3+}O_6$-octahedra form 1D chains along the c-axis by sharing edges and alkali metal ions A^+ occupy the tunnel sites in the framework formed by $M^{3+}O_6$-octahedra and BO_4-tetrahedra. Since each chain is bridged by SiO_4- or GeO_4-tetrahedra, the magnetic interchain interaction is considered to be much weaker than the intrachain interaction. Many transition metal compounds of the pyroxene family have been reported and they exhibits Néel ordered states as the ground state. Although the search for a spin-1/2 compound has been motivated by its intriguing quantum phenomena, it has been missing in the pyroxene family.

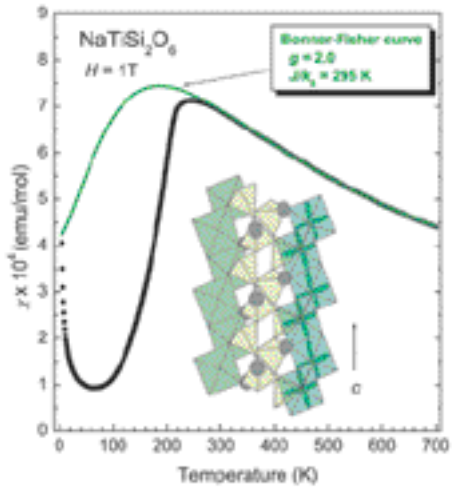

Fig.1. The magnetic susceptibility of spin-1/2 1D magnet $NaTiSi_2O_6$ is well fitted to the Bonner-Fisher equation above 250 K and at 210 K it shows a spin-Peierls-like transition. The transition, however, occurs at a temperature higher than that at the maximum point of the Bonner-Fisher curve, indicating that the intrinsic magnetoelastic instability of a 1D system cannot be considered as a driving force for the transition. The structural feature that the 1D chain is made up of skew edge-sharing $Ti^{3+}O_6$ octahedra suggests an important role of the orbital degree of freedom, that is, the orbital order on the transition.

In the present study a powder sample of $NaTiSi_2O_6$ that is a spin-1/2 compound in the pyroxene family has been successfully synthesized and a novel phase transition was found. As can be seen in Figure 1, the magnetic susceptibility (χ) is well fitted to the Bonner-Fisher equation above 250 K and rapidly decreases below 210 K. The ground state is spin-singlet. The most significant feature of this spin-Peierls-like transition is that the transition occurs at a temperature higher than that at the maximum point of the Bonner-Fisher curve. This means that the short-range magnetic correlations within the chain are not fully developed and intrinsic magnetoelastic instability of a 1 D system cannot be considered as a driving force for the transition. The structural feature that the 1 D chain is made up of *skew* edge-sharing $Ti^{3+}O_6$ octahedra (Figure 1) suggests an important role of the orbital degree of freedom, that is, the orbital order on the transition.

Principal Publication and Authors

M. Isobe, E. Ninomiya[a], A. N. Vasil'ev[b] and Y. Ueda
J. Phys. Soc. Jpn. **71** 1423-1426 (2002).
[a]Chiba University (Japan)
[b]Moscow State University (Russia)